Physiological Roles of an *Acinetobacter*-specific σ Factor

Authors and Affiliations

Emily E. Bacon[a,b], Kevin S. Myers[c,d], Rubén Iruegas-López[e], Amy B. Banta[a,c], Michael Place[c], Ingo Ebersberger[e,f,g], Jason M. Peters[a,c,h,i,j,#]

[#]Correspondence: jason.peters@wisc.edu

[a]Pharmaceutical Sciences Division, School of Pharmacy, University of Wisconsin-Madison, Madison, WI, USA

[b]Microbiology Doctoral Training Program, University of Wisconsin-Madison, Madison, WI, USA

[c]Great Lakes Bioenergy Research Center, University of Wisconsin-Madison, Madison, WI, USA

[d]Wisconsin Energy Institute, University of Wisconsin-Madison, Madison, WI, USA

[e]Institute of Cell Biology and Neuroscience, Goethe University Frankfurt, Germany

[f]Senckenberg Biodiversity and Climate Research Centre (S-BIKF), Frankfurt, Germany

[g]LOEWE Center for Translational Biodiversity Genomics (TBG), Frankfurt, Germany

[h]Department of Bacteriology, University of Wisconsin-Madison, Madison, WI, USA

[i]Department of Medical Microbiology and Immunology, University of Wisconsin-Madison, Madison, WI, USA

[j]Center for Genomic Science Innovation, University of Wisconsin-Madison, Madison, WI, USA

Keywords

ECF sigma, *relA*, small RNAs, CRISPR-associated transposons, metal stress, regulatory networks

Abstract

The Gram-negative pathogen *Acinetobacter baumannii* is considered an "urgent threat" to human health due to its propensity to become antibiotic resistant. Understanding the distinct regulatory paradigms used by *A. baumannii* to mitigate cellular stresses may uncover new therapeutic targets. Many γ-proteobacteria use the extracytoplasmic function (ECF) σ factor, RpoE, to invoke envelope homeostasis networks in response to stress. *Acinetobacter* species contain the poorly characterized ECF "SigAb;" however, it is unclear if SigAb has the same physiological role as RpoE. Here, we show that SigAb is a metal stress-responsive ECF that appears unique to *Acinetobacter* species and distinct from RpoE. We combine promoter mutagenesis, motif scanning, and ChIP-seq to define the direct SigAb regulon, which consists of *sigAb* itself, the stringent response mediator, *relA*, and the uncharacterized small RNA, "*sabS*." However, RNA-seq of strains overexpressing SigAb revealed a large, indirect regulon containing hundreds of genes. Metal resistance genes are key elements of the indirect regulon, as CRISPRi knockdown of *sigAb* or *sabS* resulted in increased copper sensitivity and excess copper induced SigAb-dependent transcription. Further, we found that two uncharacterized genes in the *sigAb* operon, "*aabA*" and "*aabB*", have anti-SigAb activity. Finally, employing a targeted Tn-seq approach that uses CRISPR-associated transposons, we show that *sigAb*, *aabA*, and *aabB* are important for fitness even during optimal growth conditions. Our work reveals new physiological roles for SigAb and SabS, provides a novel approach for assessing gene fitness, and highlights the distinct regulatory architecture of *A. baumannii*.

Importance

Acinetobacter baumannii is a hospital-acquired pathogen, and many strains are resistant to multiple antibiotics. Understanding how *A. baumannii* senses and responds to stress may uncover novel routes to treat infections. Here, we examine how the *Acinetobacter*-specific transcription factor, SigAb, mitigates stress. We find that SigAb directly regulates only a small

number of genes, but indirectly controls hundreds of genes that have substantial impacts on cell physiology. We show that SigAb is required for maximal growth, even during optimal conditions, and is acutely required during growth in the presence of elevated copper. Given that copper toxicity plays roles in pathogenesis and on copper-containing surfaces in hospitals, we speculate that SigAb function may be important in clinically-relevant contexts.

Introduction

The Gram-negative γ-proteobacterium, *Acinetobacter baumannii*, is a nosocomial pathogen with the ability to cause severe infections such as pneumonia and bacteremia (1). Its classification as an “urgent threat” to human health by the Centers for Disease Control stems from isolates that are resistant to nearly all clinically relevant antibiotics (2). At least some of this resistance can be attributed to the high abundance and activity of efflux pumps encoded in the *A. baumannii* genome (3, 4) among other resistance elements (5). Transcriptional regulation of these pumps is complex and incompletely understood (6).

Sigma (σ) factors are critical components of bacterial transcription regulation that direct RNA polymerase (RNAP) to specific promoters (7). Extracytoplasmic function (ECF) σ factors are a type of alternative σ factor that can play roles in cell homeostasis during unstressed growth but can also be activated under specific environmental conditions including envelope, oxidative, and metal stresses, among others (8-11). ECFs control downstream stress responses by directing RNAP to specialized subsets of promoters (regulon); thus, activating genes involved in mitigating the stress. Structurally, ECF σ factors contain two globular domains for binding promoter elements—σ_2 and σ_4 interact with the -10 and -35 promoter elements, respectively—and require near-consensus promoters due to their reduced capacity for promoter melting (12, 13).

RpoE is one of the most extensively studied ECFs (14, 15). In *Eschericha coli*, the RpoE signal transduction pathway is activated upon detecting envelope stress in the form of misfolded

outer membrane proteins or lipopolysaccharide (LPS) intermediates. These molecules are recognized by periplasmic proteases or the anti-σ RseB which accelerates proteolysis of the anti-σ RseA, releasing RpoE to transcribe its regulon (16, 17). The RpoE regulon includes over 100 protein coding genes as well as 3 non-coding RNAs that are critical to its envelope homeostasis function (18-20). Many γ-proteobacteria, such as *Pseudomonas aeruginosa* and *Vibrio* species, contain a homolog of RpoE, which recognize similar promoter sequences and regulate overlapping sets of genes (e.g., LPS transport and outer membrane repair genes) (21-24). *A. baumannii* strains contain ECF sigma factors (25), but their functions are poorly characterized. Despite the importance of RpoE to envelope homeostasis in γ-proteobacteria, it is unclear if any ECF σ factors in *A. baumannii* play similar roles.

Gene regulatory patterns and regulators in *A. baumannii* are often distinct from those observed in model organisms, such as *E. coli* K-12. For example, *A. baumannii* lacks homologs of key stress response genes including the general stress response σ factor RpoS and the Rcs envelope stress signal transduction system (26, 27). Instead, *A. baumannii* encodes the two-component system BfmRS that exhibits phenotypic overlap with Rcs and other envelope stress responses (27, 28). Additionally, *A. baumannii* contains numerous genes of unknown function, including putative transcription factors and cell envelope genes (25, 29). *A. baumannii* can survive a wide range of stresses including prolonged desiccation on surfaces, metal toxicity and oxidative stress during host infection, and evading antibiotic killing (30-32). However, little is known if *A. baumannii* ECF σ factors play a role in mitigating these stresses.

Here, we investigate the regulon and physiological roles of an *Acinetobacter*-specific ECF σ factor we call, “SigAb”. The gene encoding SigAb (ACX60_04565 in ATCC 17978) has been annotated as "RNA polymerase sigma factor", or "*sigX*", and was suggested to be similar to RpoE and the *Pseudomonas* homolog, AlgU, based on the small number of residues that align in predicted σ_2 and σ_4 domains (25). We find that SigAb recognizes a distinct DNA binding site and regulon from RpoE, and we show that SigAb instead has roles in metal resistance and

104 general fitness during growth without added stressors. Finally, we discuss the implications of our
105 work for gene regulation in *Acinetobacter* species.
106
107 **Results**
108 **SigAb is an *Acinetobacter*-specific σ factor**
109 We first sought to compare SigAb to characterized ECF σs, including RpoE. As
110 expected, a search for proteins with similar predicted folds using Phyre2 (33) returned high-
111 confidence matches to structurally characterized ECFs (Fig. S1). Further, we were able to
112 model SigAb in place of *E. coli* RpoE in an RpoE-RNAP holoenzyme structure (Fig. S2 (34)).
113 However, SigAb showed low overall primary sequence identity to *E. coli* RpoE (18%), the RpoE
114 ortholog in *P. aeruginosa* AlgU (19%), and the *P. aeruginosa* ECF SigX (20%), and key DNA
115 binding residues in RpoE differed in SigAb (e.g., RpoE F64, R76, S172, F175, etc.), suggesting
116 distinct interactions with promoter DNA.
117 The low sequence identity between RpoE and SigAb left their precise evolutionary
118 relationships unclear. To further shed light on the evolutionary trajectory that gave rise to these
119 sequences, we determined the phylogenetic profiles of SigAb and RpoE using a targeted
120 ortholog search. Interestingly, this suggested at first sight that RpoE and SigAb are indeed
121 orthologs as their phylogenetic profiles contain, in part, the same proteins. To test this
122 hypothesis further, we created a non-redundant protein list from the two profiles and selected a
123 representative set covereing the γ-proteobacterial orders. A subsequent multiple sequence
124 alignment revealed a conspicuous conservation pattern (Fig. 1a). Sequences from a diverse set
125 of orders including the Enterobacterales, Vibrionales, Pseudomonadaceae, Pasteurellales, and
126 Alteromonadales are highly conserved; Among these sequences, we find RpoE of *E. coli.*
127 Moraxellaceae—and in particular members of the genus *Acinetobacter*—formed a separate
128 group of sequences including SigAb whose conservation pattern is clearly distinct from RpoE
129 (Fig. 1a). We next constructed a phylogenetic tree based on our alignment (Fig. 1b). We found

that the conservation pattern seen in the multiple sequence alignment is reflected in the tree topology. Sequences from different γ-proteobacterial orders are grouped into one clade to the exclusion of the representatives from the genus *Acinetobacter.* This placement is at odds with the accepted evolutionary relationships of the organisms where the Moraxellales are considered the next relatives of the Pseudomonadales. It strongly suggests that SigAb in *Acinetobacter* represents a distinct evolutionary lineage from that of RpoE. Furthermore, RpoE-like ECFs are absent from the *Acinetobacter* genomes we queried, including *A. baumannii* and other members of the *A. calcoaceticus-baumannii* (ACB) complex. Taken together, SigAb is an ECF σ factor found in *Acinetobacter* species that is evolutionarily distinct from RpoE.

SigAb-dependent promoters are distinct from those recognized by RpoE

Protein modeling and evolutionary analysis highlighted distinctions between RpoE and SigAb, raising the possibility that SigAb could recognize a different promoter sequence. Because ECF σ factor expression is often autoregulated, we investigated the DNA sequence upstream of *sigAb* for a possible SigAb promoter. Indeed, we found an upstream sequence that was specifically recognized by SigAb (P_{sigAb}) (Fig. 2). To map P_{sigAb}, we used 5′ RACE to determine the 5′ end of the *sigAb* transcript (Fig. S3a). We next aligned the DNA sequence upstream of the putative P_{sigAb} transcription start site (TSS) across selected *Acinetobacter* species, finding highly conserved motifs that could potentially serve as promoter -10, -35, and UP elements (35) (Fig. S3b). To test for SigAb-dependent promoter activity, we cloned the putative P_{sigAb} sequence upstream of a Red Fluorescent Protein reporter gene (*mRFP*) and integrated the reporter into the genomes of *A. baumannii*, which contains a native copy of *sigAb*, and *E. coli*, which lacks *sigAb* (Fig. 2a). We found that overexpression (OE) of SigAb from a multi-copy plasmid increased reporter activity by >150-fold in *A. baumannii* (Fig. 2b) and that the presence of the *sigAb* gene was necessary and sufficient for P_{sigAb} reporter activity in *E. coli* (Fig. 2c). The absence of reporter activity in *E. coli* lacking *sigAb* suggests that RpoE does not

recognize P_{sigAb} (Fig. 2c). Further, a P_{rpoE} reporter showed activity in *E. coli*, but not *A. baumannii* (Fig. S4), supporting that SigAb does not recognize RpoE-dependent promoters.

With a validated reporter in hand, we sought to determine which bases within P_{sigAb} are important for SigAb activity. Conserved positions in our P_{sigAb} alignment across *Acinetobacter* species provided a starting point for systematic mutagenesis of the promoter sequence. Using our P_{sigAb} reporter, we comprehensively mutated individual bases in the putative -10 and -35 elements and measured reporter expression in *A. baumannii*; this allowed us to identify the key bases for promoter activity (Fig. 2d and S5a). We weighted P_{sigAb} variants by promoter activity and created a SigAb activity logo, which revealed distinct -10 and -35 elements (Fig. 2e). The core SigAb -10 (CGTT) and -35 (GTCAAC) identified by our mutagenesis approach differ from those determined by promoter alignments for RpoE (-10 ~TCAAA and -35 ~GGAACTT (19)). Other promoter features also contributed to P_{sigAb} activity. P_{sigAb} has a 17-bp spacer sequence between the -10 and -35; reducing the spacer length to 16 had little impact on activity but increasing the spacer length to 18 reduced activity by ~3-fold (Fig. S5b). Our P_{sigAb} alignment also suggested that a conserved run of four T bases in the spacer could impact activity. Consistent with this, we found a modest 2.5-fold reduction in activity when all four T bases were substituted with G bases (Fig. S5c). Finally, a run of A/T bases upstream of the -35 may serve as an UP element, as substitution of this sequence with random bases reduced P_{sigAb} activity by 10-fold (Fig. S5c). In sum, we identified a SigAb-dependent promoter, systematically defined a promoter activity motif with key sequences required for activity, and showed that this promoter is distinct from that of RpoE.

SigAb directly controls a small regulon

As the SigAb regulon remained uncharacterized, we set out to identify direct targets of SigAb, taking a two-pronged approach: 1) we scanned the *A. baumannii* ATCC 17978 genome for putative SigAb binding sites that matched our promoter activity motif, and 2) we performed

chromatin immunoprecipitation followed by sequencing (ChIP-seq) to find DNA sites occupied by SigAb in whole cells. We found that SigAb directly controls a small regulon of genes that includes one or more non-coding RNAs. We first scanned the ATCC 17978 genome for exact matches to the P_{sigAb} -10 (CGTT) and -35 (GTCAAC) elements with spacer lengths between 16 and 18 bases. We identified a total of 17 motifs (Fig. S6a); surprisingly only three were upstream of annotated protein coding genes in an orientation that would be expected to drive downstream transcription. We individually cloned the 17 motifs into our mRFP reporter construct, finding that many of the motifs had substantial activity upon SigAb OE from a multi-copy plasmid (Fig. S6b). In addition to P_{sigAb}, SigAb-dependent promoters were identified upstream of the gene encoding the (p)ppGpp synthetase, *relA*, a global regulator during nutrient limitation (36-38) as well as the sulfate transporter operon, *cysTW*. We found another highly active SigAb-promoter upstream of a putative small RNA (sRNA) that had previously been identified by sequencing of RNAs (RNA-seq), but the promoter for this sRNA had not been characterized (39). We call this sRNA "*sabS*" for SigAb-dependent sRNA. Importantly, the *sigAb*, *relA*, and *sabS* promoter motifs exhibit significantly greater SigAb-dependent activity than the other putative motifs (Fig. S6b).

We next used ChIP-seq to identify SigAb binding sites in whole cells grown in rich medium. For this purpose, we generated an N-terminally Halo-tagged variant of SigAb that we confirmed retained activity using our P_{sigAb} reporter (Fig. S7). Halo-tagged proteins covalently bind Halolink resin, enabling stringent washing conditions that remove non-specific DNA (40). Peak calling analysis of three independent ChIP-seq samples showed only three sites that were both significantly enriched across at least two replicates and also contained a putative *sigAb* promoter motif (Fig. 3a, Table S5). These three enriched sites were in front of the following genes: 1) *sigAb* (Fig. 3b), 2) *relA* (Fig. 3c), and 3) *sabS* (Fig. 3d). Although *sigAb* and *sabS* showed much stronger ChIP-seq signal than *relA*, all three motifs exhibited similar induction upon plasmid-based SigAb OE in our mRFP reporter assay (Fig. 3e and Fig. 2b). We conclude

208 that SigAb directly controls a small regulon including itself, *relA*, and one or more non-coding
209 RNAs.
210
211 **SigAb indirectly affects global transcription**
212 SigAb control of the global regulator *relA* and putative sRNAs raised the possibility that
213 increases in SigAb activity could affect transcription beyond its small, direct regulon. To test for a
214 global effect of SigAb on transcription, we overexpressed *sigAb* from the IPTG-inducible *trc*
215 promoter on a multi-copy plasmid and performed an RNA-seq timecourse post induction (Fig.
216 4a). Interestingly, hundreds of genes increased in expression by 1 hour post *sigAb* induction
217 compared to a vector only control (Fig. 4b). After only 5 minutes of induction, 125 genes had
218 increased expression by over 2-fold (FDR < 5%), suggesting that upregulation of these genes is
219 a secondary effect of SigAb OE (Fig. S8a). Gene set enrichment analysis showed that a variety
220 of cellular pathways were upregulated at the 5 min timepoint including "metabolism and
221 oxidoreductase activity," which contained *relA* among other metabolic genes and "membrane
222 and regulation of cellular processes" in addition to TetR and LysR-type transcription factors
223 which may partially explain the large number of genes affected by 60 min (Fig. 4c); however,
224 these upregulated genes lacked known RpoE targets. Although not a defined enrichment group,
225 we note that many prophage genes (20 genes) were upregulated by SigAb OE (identified using
226 Phaster (41)), which may be due to stress-induced prophage expression. The vast majority of
227 these upregulated genes had no associated SigAb binding site, suggesting a widespread
228 indirect effect of SigAb OE.
229 Two enriched groups of SigAb upregulated genes contained transporter-encoding genes
230 with possible relevance to *A. baumannii*'s resistance and pathogenesis lifestyles (Fig. 4d).
231 These groups included the RND multidrug efflux transporter AdeA/AdeB and the CusA family
232 heavy metal efflux RND transporter. The only gene in this group with an upstream SigAb

promoter motif is the sulfate transporter CysW, suggesting indirect regulation for most of these RND efflux transporters.

In fact, among the 17 SigAb promoter motifs validated by our reporter assay, only 6 were upregulated upon SigAb OE: *sigAb* and two downstream genes that we predict form an operon, *relA*, *cysT* and downstream gene *cysW* that form an operon, and three putative sRNAs including *sabS* (Fig. S8b). We speculate that SigAb promoters that show activity in our reporter assay but lack RNA-seq signal may produce untranslated RNAs in their native context that are subject to termination and rapid degradation (42).

We reasoned that indirect effects of SigAb overexpression could be attributable to increased levels of the global regulator, RelA. To test this hypothesis, we overexpressed RelA from a strong, IPTG-inducible promoter on a multi-copy plasmid and performed RNA-seq after 10 min of induction. Although RelA OE caused significant upregulation of 62 genes, most of the genes did not overlap with those increased upon SigAb OE (Fig. S9). Therefore, the large, indirect effect of SigAb on global transcription is not through regulation of *relA*, at least under the conditions tested.

SigAb mitigates and responds to copper stress

Upregulation of predicted heavy metal and copper transporters upon SigAb OE (Fig. 5a) suggested that SigAb could be involved in resistance to metal toxicity. Indeed, disruption of *sigAb* was found to sensitize cells to excess copper and zinc in a transposon sequencing (Tn-seq) screen of *A. baumannii* ATCC 17978 (43). To validate and extend these findings, we generated a CRISPR interference (CRISPRi) knockdown strain of *sigAb* in *A. baumannii* ATCC 19606 and phenotyped it in various transition metals. We found that *sigAb* knockdown sensitized cells to copper and nickel toxicity (Fig. 5b and S10a). We first tested liquid medium growth of the *sigAb* knockdown strain in elevated copper and nickel, finding that *sigAb* showed reduced growth relative to the non-targeting control in both conditions. To expand our

phenotyping to additional conditions (e.g., manganese, cobalt), we tested growth of the *sigAb* knockdown in Biolog Phenotype Microarray (PM) plates (Fig. 5c and S10b). The PM plates recapitulated our copper and nickel results but showed no additional phenotypes. This suggests that the SigAb-dependent metal resistance is restricted to certain transition metals.

As small RNAs are often global regulators, we reasoned that *sabS* could be playing a role in this SigAb-dependent metal resistance. We constructed a *sabS* CRISPRi knockdown strain in *A. baumannii* ATCC 19606 and phenotyped it using Biolog PM plates. Indeed, we found that the *sabS* KD strain is sensitive to both copper and nickel stress, similar to the *sigAb* KD strain (Fig. S10c). Because SigAb activates *sabS* expression (Fig. S6b), we suggest that *sabS* is either directly or indirectly modulating SigAb-dependent metal resistance effects.

Given the role of SigAb in metal resistance, we considered that elevated metal levels could directly or indirectly stimulate SigAb activity. To test this hypothesis, we measured the activity of our P_{sigAb} mRFP reporter under metal stress conditions using Biolog PM plates. We found that copper stress increased SigAb activity by ~2.5-3.5-fold relative to a constitutive promoter, depending on cell density (Fig. S11a). By contrast, other metals and conditions failed to stimulate P_{sigAb} activity above basal levels (Fig. 5d and S11b). Taken together, we conclude that SigAb activity is required for copper resistance and that SigAb responds to copper stress.

Members of the *sigAb* operon, *aabA* and *aabB*, have anti-σ activity

We found that *sigAb* forms an operon with two uncharacterized downstream genes we call *aabA* (anti-SigAb A, ACX60_04560 in ATCC 17978) and *aabB* (anti-SigAb B, ACX60_04555 in ATCC 17978), as the coding sequences for *sigAb-aabA* and *aabA-aabB* overlap and *sigAb-aabA-aabB* are co-regulated by SigAb in our RNA-seq data (Fig. S8b). Anti-σ factors are often co-transcribed in operons with their cognate ECF σs, forming a negative regulatory loop that prevents toxicity from runaway positive autoregulation by the ECF (12). For instance, *rpoE* exists in an operon with genes that encode the anti-RpoE factor, RseA, and the RseA stabilizing

protein, RseB. RseA binds to RpoE and anchors it to the membrane while RseB binds to RseA and stabilizes it against degradation by membrane proteases under non-inducing conditions (17, 44). Consistent with an RpoE-type regulation scheme, the predicted localizations of SigAb, AabA, and AabB are cytoplasmic, transmembrane, and periplasmic, respectively (Fig. S12a and S12b). We used Alphafold multimer to predict possible interactions between SigAb, AabA, and AabB, finding that AabA could bind to both SigAb and AabB *in silico* (Fig. 6a). AabB was predicted to fold around the periplasmic end of AabA, adopting a tighter alpha-helical structure than when modeled alone (Fig. S12c). AabA modeling showed a distinct interaction with SigAb compared to the interaction of RpoE and RseA, which was expected given that AabA is a much smaller protein than RseA (107 aa versus 217 aa, respectively) (Fig. 6b). Interestingly, the AabA-SigAb interaction is similar to that of the anti-sigma CnrY with sigma CnrH, a cobalt-nickel resistance regulator from the β-proteobacterium *Cupriavidus metallidurans* (Fig. 6b, (45)).

To test for anti-SigAb activity, we overexpressed AabA and AabB, either individually or in combination, in an *A. baumannii* strain containing our P_{sigAb} mRFP reporter; this strain also contained the wild-type *sigAb-aabA-aabB* operon at its native locus (Fig. 6c). We found that all OE strains showed significant reduction of SigAb activity, and that activity was reduced to a similar level across strains. Although it was clear from this result that OE of *aabA*, *aabB*, or both caused anti-SigAb activity, the presence of native copies of both genes complicated interpretation of their biological roles. To eliminate interference in our assay by native *A. baumannii* proteins, we heterologously expressed SigAb, AabA, AabB and combinations thereof in an *E. coli* strain containing our P_{sigAb} mRFP reporter (Fig. S12d). We found that co-expression of AabA and AabB significantly reduced P_{sigAb} activity, consistent with our RpoE-like model of anti-σ function. Expressing the cytoplasmic domain of AabA alone resulted in potent inhibition of SigAb activity, demonstrating that periplasmic localization is not required for AabA activity. Unexpectedly, we observed a significant reduction in SigAb activity when AabB was expressed alone, suggesting additional complexity to AabA-AabB anti-σ function beyond the *rpoE*

311 paradigm. We conclude that AabA and AabB have anti-SigAb functions, although their precise
312 mechanisms remain unknown.
313
314 **Targeted Tn-seq reveals that the *sigAb* operon is required for fitness in rich medium**
315 The physiological importance of genes in the *sigAb* operon under standard growth
316 conditions is largely unknown. Tn-seq studies of *A. baumannii* ATCC 17978 and AB5075 have
317 described *sigAb* and *aabB* as non-essential and *aabA* as essential (29, 46), and a Tn disruption
318 of *sigAb* was recovered in the ordered AB5075 mutant library. However, genome-scale Tn-seq
319 studies can have limited resolution at the single gene level—especially for short genes (47).
320 Moreover, arrayed mutant libraries can accumulate secondary mutations during passaging that
321 alter phenotypes (48). To better understand the physiological roles of *sigAb* operon genes and
322 to establish a higher-resolution approach to gene phenotyping, we employed a CRISPR-
323 associated transposon (CAST) system to programmatically disrupt target genes we call,
324 "CRISPRt". Our previously developed CRISPRt system (49) uses vectors that do not replicate in
325 recipient bacteria to transiently express *cas* and *tns* genes from the well characterized *Vibrio*
326 *cholerae* CAST (*Vc*CAST) and guide RNAs (gRNAs) with spacers that match target genes. The
327 Cas-Tns-gRNA complex binds to target DNA complementary to the spacer (protospacer), then
328 inserts DNA between Tn*6677* ends ~49 bp downstream of the protospacer (Fig. 7a). Because
329 the delivery vectors are non-replicative, insertion of Tn*6677* can be directly selected for using an
330 antibiotic marker, similar to standard Tn-seq libraries using Tn*5* or *mariner*. We previously
331 demonstrated that CRISPRt could inactivate reporter genes in *E. coli* K-12 (49). To establish
332 that CRISPRt could be used for targeted Tn-seq in *A. baumannii*, we made pooled libraries of
333 gRNA spacers targeting known non-essential (*rpoN*) and essential (*rpoD*) genes (Fig. 7b). As
334 expected, we were able to disrupt the non-essential *rpoN* gene with Tn*6677* insertions across
335 the entirety of the coding sequence. By contrast, targeting of the essential *rpoD* gene only

allowed for insertions flanking the coding sequence, validating CRISPRt targeted Tn-seq as a high-resolution approach to determine gene essentiality in *A. baumannii*.

We next used CRISPRt to investigate essentiality of the *sigAb* operon. We tiled all three genes in the *sigAb* operon with targeting spacers as well as a predicted non-essential upstream gene (ACX60_04570) as a control. We found that Tn*6677* could be inserted across the operon, but we obtained far fewer reads from Tn insertions in *sigAb*, *aabA*, and *aabB* relative to the control gene (Fig. 7c and Fig. S13). Reduced reads from *sigAb* operon insertions could be attributed to reduced fitness of Tn insertion mutants or lower CRISPRt guide efficacy for spacers targeting the *sigAb* operon. To disambiguate these two possibilities, we performed CRISPRt Tn-seq assays on strains with a second copy of either *sigAb* or *sigAb-aabA-aabB* transcribed from their native promoter and integrated in single copy at the att_{Tn7} locus (Fig. 7c and Fig. S13). *Trans* complementation of *sigAb* resulted in a substantial increase in *sigAb* Tn insertion reads (>30-fold) but reads for Tn insertions in *aabA* or *aabB* remained low. *Trans* complementation of the entire *sigAb* operon resulted in increased Tn-seq reads across all three genes (>30-fold), ruling out low efficiency of CRISPRt gRNAs as an alternative hypothesis. We conclude that genes in the *sigAb* operon, while not strictly essential, are required for fitness even in the absence of metal stress.

Discussion

Elucidating the regulatory pathways by which bacterial pathogens mitigate stress may reveal new weaknesses that can be exploited by future treatments. This work substantially advances our understanding of gene regulation in the Gram-negative pathogen, *A. baumannii*, by defining the physiological roles of the ECF σ factor, SigAb. We find that SigAb is *Acinetobacter*-specific (Fig. 1) and determine that the promoter sequences it recognizes are distinct from other, well characterized σ factors (Fig. 2). By identifying SigAb direct binding sites (Fig. 3) and changes in the transcriptome during SigAb overexpression (Fig. 4), we establish a

small direct and a large indirect regulon. We show that SigAb function is required for resistance to excess copper and that SigAb activity is stimulated by copper (Fig. 5), suggesting a coherent regulatory scheme for mitigating copper stress. Finally, we demonstrate that downstream genes in the *sigAb* operon have anti-SigAb activity (Fig. 6) and that disruption of any member of the *sigAb* operon leads to reduced fitness in rich medium (Fig. 7). Our work supports a growing body of literature that distinguishes regulatory strategies used by *A. baumannii* from well-studied Gram-negatives, such as *E. coli* and *P. aeruginosa*. Such distinctions may be relevant in the search for *A. baumannii*-specific treatments.

Our results further highlight fundamental differences in gene regulation strategies employed by *A. baumannii* versus related, Gram-negative pathogens. Despite previous annotations based on extrapolations from *E. coli* and *P. aeruginosa* (25), we definitively show that the only ECF σ factor present in many strains of *A. baumannii*, SigAb, is not RpoE. Both the SigAb promoter and regulon are distinct from RpoE, and RpoE-dependent promoters from *E. coli* are inactive in *A. baumannii*. Taken together with the fact that *A. baumannii* lacks other conserved σ factors, including RpoS, our results and the work of others (26, 27, 43) point to a global rewiring of gene regulatory networks that occurred sometime between the last common ancestor of *P. aeruginosa* and *A. baumannii*. As RpoE has a large, conserved direct regulon in many γ-proteobacteria (18, 22, 50, 51), and conserved genes that are part of the RpoE regulon in *E. coli* and *P. aeruginosa* are not controlled by an ECF σ in *A. baumannii*, other transcription factors must control the outer membrane stress response in *A. baumannii*. The BfmRS two-component system is one such player (27, 28), but other systems are likely involved that have not been described to date and warrant future studies.

The direct regulon of SigAb seems to contain only a handful of genes, which is consistent with many other ECF σ factors (but not RpoE) (51). By the conservative criteria applied here—namely, that direct targets must have promoter motifs, ChIP binding sites, and be upregulated by SigAb overexpression—we find only three direct targets. Autoregulation of the

388 *sigAb-aabA-aabB* operon at the transcriptional level is a hallmark of ECF σ factors (8, 51), and
389 the presence of a negative feedback loop consisting of an anti-σ factor is also commonplace
390 (12, 52). The smaller size of AabA compared to RseA and substantial anti-σ activity of the AabA
391 cytoplasmic fragment raise questions about AabA proteolysis and release of SigAb, possibly
392 due to a copper stimulus. Direct control of the stringent response factor, *relA* (37), by SigAb has
393 unknown functional consequences. RNA-seq of RelA or SigAb overexpressing strains showed
394 little overlap, seemingly ruling out increased RelA/(p)ppGpp as a cause of the indirect regulon.
395 However, there may be other conditions in which the regulatory relationship between SigAb and
396 RelA plays a functional role, such as during metal stress in the host environment. Another host-
397 associated pathogen, *Mycobacterium tuberculosis*, also uses an ECF σ factor to control
398 expression of *relA* (53, 54), suggesting a functional convergence between these two unrelated
399 pathogens. Finally, we show that SigAb directly regulates the putative small RNA, *sabS*. This
400 sRNA was previously detected in a transcriptome study (39), but its dependence on SigAb was
401 unknown until our work. A recent preprint displaying GRIL-seq data in *A. baumannii* suggests
402 that the downregulated genes in our *sigAb* overexpression RNA-seq dataset are direct targets
403 of *sabS*, however these genes are mostly unannotated, hypothetical proteins (55). sRNAs are
404 often core members of ECF σ regulons (56, 57). By example, the essential function of RpoE in
405 *E. coli* is to transcribe three sRNAs that downregulate key envelope target genes (20, 58). Of
406 the direct SigAb targets, SabS is most likely to be responsible for the changes seen in the
407 indirect regulon, given that *sabS* and *sigAb* knockdowns show similar phenotypes. However,
408 how SabS can increase the expression of hundreds of genes is unknown and may be due to
409 additional, indirect regulation.

410 The indirect regulon of SigAb is critical to its physiological roles. Our phenotyping
411 experiments point to SigAb, and by extension, SabS, as important mediators of the metal stress
412 response, and we find that SigAb indirectly regulates several heavy metal RNA efflux pumps.
413 Metal stress and acquisition is key to pathogenesis by *A. baumannii* and, thus, SigAb may be

414 important under those conditions. The levels of transition metals, such as copper and
415 manganese, are tightly regulated during growth in the host environment, as bacteria require
416 metals for viability but metals are toxic in excess (59, 60). Copper may be relevant for other
417 clinical settings as it is often used as a bactericide due to its high toxicity to bacteria (61). *A.*
418 *baumannii* is known to evade copper toxicity via several gene clusters including the resistance
419 genes, *copA*/*copB*, (62) as well as the histidine kinase-response regulator pair, *cusRS* (63);
420 these genes are also part of the SigAb indirect regulon. Interestingly, SigAb is distinct from other
421 copper responsive ECF σ factors that use an anti-σ-independent mechanism for signal
422 transduction (ColE-like ECFs) or through activation of carotenoid genes in response to copper
423 stress (CarQ-like ECFs) (64). Taken together, the role of SigAb in mitigating metal stress
424 underscore its importance to *A. baumannii* physiology and potentially pathogenesis.
425 In this study, we used a targeted version of Tn-seq called “CRISPRt” to characterize
426 gene fitness and essentiality. CRISPRt has advantages for probing the essentiality of subsets of
427 genes that may be broadly applicable. For instance, Tn-seq using pseudo-random insertions
428 (e.g., Tn*5*) often fails to achieve high-density coverage of specific loci unless very large insertion
429 libraries are constructed. The need to construct such libraries typically precludes the use of
430 genetic complementation in the context of Tn-seq; however, CRISPRt targeting of specific loci
431 makes Tn-seq complementation possible with small libraries. Targeted, CRISPRt follow-ups of
432 specific loci could provide a way to validate essential gene calls from pseudo-random Tn-seq at
433 scale, which would be especially valuable for non-model bacteria. Importantly, our CRISPRt
434 analysis had sufficient resolution to determine that members of the *sigAb* operon had reduced
435 fitness, in contrast to other studies that made binary essential/non-essential calls (29, 46). As
436 with pseudo-random transposition, polar effects onto downstream genes from changes in
437 transcription are a concern, but the possibility of complementation mitigates that issue, and the
438 trade-off may be worthwhile for large-scale studies validating dozens of genes at a time.

Demonstrating CAST-based, targeted Tn insertion in *A. baumannii* adds another genetic tool for gene phenotyping to this urgent threat pathogen.

Materials and Methods

Strains and growth conditions. Strains are listed in Table S1. *Escherichia coli* K-12 and *Acinetobacter baumannii* (strains ATCC 17978-UN or ATCC 19606) were grown in Lennox lysogeny broth (LB) at 37°C shaking in a flask at 250 rpm, in a culture tube on a rollerdrum at max speed, in a 96-well plate shaking at 900 rpm, or in a plate reader shaking (Tecan Infinite Mplex, Infinite Nano+, or Sunrise). Culture medium was solidified with 1.5% agar for growth on plates. Where noted, *A. baumannii* strains were grown in EZ Rich Defined Medium (Teknova M2105), following manufacturer's recipe except supplemented with 40 mM succinate instead of glucose (AbRDM). Antibiotics were added when necessary: 100 µg/mL ampicillin (amp), 30 µg/mL kanamycin (kan), 50 µg/mL apramycin (apr), 50 µg/mL spectinomycin (spec) for *E. coli* and 150 µg/mL carbenicillin (carb), 60 µg/mL kanamycin (kan), 100 µg/mL apramycin (apr), 150 µg/mL gentamycin (gent) for *A. baumannii*. Diaminopimelic acid (DAP) was added at 300 µM to support growth of *E. coli* dap- donor strains. IPTG (isopropyl b-D-1-thiogalactopyranoside) was added at 0 to 1 mM as indicated in the figures or figure legends. Strains were preserved in 15% glycerol at -80°C. Plasmids were propagated in *E. coli* strain BW25141 att_{Tn7}::*acrIIA4* (sJMP3053) for DNA extraction and analysis or in *E. coli* strain WM6026 att_{Tn7}::*acrIIA4* (sJMP3257) for conjugation.

General molecular biology techniques. A complete list of plasmids and oligonucleotides are listed in Tables S2 and S3. Oligonucleotides were synthesized by Integrated DNA Technologies (Coralville, IA). Genomic DNA was purified using GeneJet Genomic DNA kit (Thermo K0503). Plasmid DNA was purified using the GeneJet Plasmid Miniprep kit (Thermo K0503) or the Purelink HiPure Plasmid Midiprep kit (Invitrogen K210005). PCR was performed according to

manufacturer directions using Q5 or OneTaq DNA Polymerases (NEB, Ipswitch, MA). DNA was digested with restriction enzymes from New England Biolabs (NEB). PCR products were purified with DNA Spin and Concentrate kit (Zymo Research, Irvine, CA, D4013 or NEB Monarch, T1030) following manufacturer instructions or gel-purified from kit (Zymo Research). Plasmids were assembled using NEBuilder HiFi DNA assembly kit (NEB). DNA was quantified on a Nanodrop Lite or Qubit HS DNA or RNA kit (Thermo). Plasmids were transformed into electrocompetent *E. coli* cells using a 0.1 cm cuvette (Fisher FB101) and a BioRad Gene Pulser Xcell (25 µF, 200 ohm, 1800 V). Plasmids and recombinant strains were sequenced via Sanger sequencing by Functional Biosciences or Oxford Nanopore sequencing by Plasmidsaurus. Next-generation sequencing was performed by the UW-Madison Biotechnology Center Next Generation Sequencing Core using an Illumina NovaSeq 6000 or Azenta using an Illumina MiSeq.

SigAb structural modeling. The SigAb protein sequence was structurally modeled using Phyre2 “Normal” setting to identify proteins with similar structures (See Fig. S1). To model based off of *E. coli* RpoE specifically, Phyre2 was used with “one-to-one threading” (33). Structural model was traced onto RpoE holoenzyme crystal structure (34) in PyMOL.

Evolutionary analysis of SigAb. SigAb targeted ortholog search and phylogentic analyses were constructed similar to that previously described (65). Briefly, 2822 γ-proteobacteria genome assemblies were retrieved from the RefSeq database (release 213, downloaded on September 2022), selecting reference genomes and isolates of interest, including 196 isolates from the *Acinetobacter* genus. To perform phylogentic profiling, protein reference sequences of RNA polymerase sigma factors were selected from *Acinetobacter baumannii* ATCC 19606 (WP_000362312.1) and *Escherichia albertii* Sample 167 (WP_001295364.1). Phylogenetic profiles were computed using fDOG 0.1.23 (https://github.com/BIONF/fDOG) with the following

parameters: compilation of 35 core orthologs selected with a taxonomic distance minimum of genus and maximum of class.nHomologous sample protein sequences were aligned with MAFFT (66) and reconstructed into a phylogeny using FastTree (67). Aligned sequences were classified into clades in a phylogenetic-aware manner using Fastbaps (68).

5' RACE. The 5' end of the sigAb transcript was identified using 5' RACE following manufacturer's protocol with template switching RT enzyme mix (NEB; M0466). Briefly, cDNA from *A. baumannii* ATCC 17978 RNA was made using RT oligo oJP2139 and template-switching oligo oJMP2131. 5' region of sigAb transcript was amplified with oJMP2130/oJMP2138 using NEBNext Ultra II Q5 master mix and touchdown PCR, spin purified with DNA clean and concentrate kit (NEB), and sequenced with Plasmidsaurus.

Promoter activity fluorescent assays. Putative P_{sigAb} motifs were cloned into Tn*7*-based mRFP reporter vectors using annealed oligos and ligation of 54 bp promoter motifs into BsaI-cut vector (pJMP3570). These promoter reporters were integrated onto the chromosome in the att_{Tn7} site in sJMP3075 (*E. coli* MG1655 WT), sJMP3348 (*A. baumannii* ATCC 17978 WT), and sJMP3329 (*A. baumannii* ATCC 19606 WT) by tri-parental Tn*7*-mediated conjugation with the transposase vector-containing donor strain, sJMP3261. Strains were grown in AbRDM in a 96-well plate overnight to saturation and red fluorescence and OD_{600} were measured in a Tecan Infinite Mplex or Nano+ plate reader.

Promoter Mutagenesis Screen. A P_{sigAb} mutation library containing 54 bp promoter region with individual point mutations in putative -10 and -35 motifs, and chunk mutations in putative UP element and spacer region T-tract, was constructed as follows. An oPool (oJMP2304) containing 66 oligos with the mutated promoter region was amplified with oJMP463/oJMP464 using low-cycle Q5 PCR with the following conditions: 98°C 30s; 98°C 15s, 56°C 15s 72°C 15s, 16 cycles;

72°C 5 min. PCR product was spin-purified, quantified with nanodrop, digested with PacI/SpeI, ligated into PacI/SpeI-digested pJMP3539, and transformed into the mating strain to make sJMP3544 containing the P_{sigAb} mutation library. The PsigAb library was integrated into the attTn7 site in *A. baumannii* ATCC 19606 by quad-parental mating with sJMP3329 (WT *A. baumannii*) + sJMP4061 (helper plasmid) + sJMP3261 (Tn*7* transposase) + sJMP3544 (P_{sigAb} mutation library) and selection with apr. Isolated colonies were picked into 3 96-well plates, grown up in LB + apr overnight to saturation, and stored as sJMP3565, sJMP3566, and sJMP3567.

To determine the identity of each promoter mutation in each well, barcoded colony PCR followed by sequencing was performed as follows. Cells in each 96-well plate were diluted 1:100 and 2 µL were added to OneTaq PCR mix with oJMP2292/oJMP1678-1773 containing 6 nt defined barcodes. Barcoded PCR products from each plate were pooled together, spin purified, and sequenced. The identity of each mutation in each well was decoded using the barcodes as a key. Once the identity of each well was found, the P_{sigAb} promoter activities were determined by growing up the 96-well plates in AbRDM to saturation and quantifying red fluorescent protein normalized to OD_{600} in a Tecan Mplex. The median activity for each mutation was compiled into an activity logo using WebLogo sequence logo generator (69).

Chromatin Immunoprecipitation-sequencing (ChIP-seq). An expression vector harboring N-terminally tagged SigAb was constructed by amplifying HaloTag (HT) gene from sJMP3331 gDNA using oJMP2295/oJMP2296 with a gly-ser-gly-ser flexible linker and no translation stop codon, amplifying *sigAb* from sJMP3348 gDNA using oJMP2294/oJMP1905, and HiFi assembling into NcoI/BamHI-digested pJMP3653 expression vector containing a strong, IPTG-inducible promoter (70) to make pJMP3571. pJMP3571 was electroporated into the mating strain (sJMP3257) to make sJMP3575. To make an *A. baumannii* ATCC 17978 strain containing

the HT-SigAb expression vector (kanR), sJMP3575 was mated with sJMP3348 to make sJMP3584.

ChIP-seq on sJMP3584 was performed in triplicate as described previously (40, 71). Briefly, cells were grown in 100 mL AbRDM + 70μM IPTG + kanamycin to maintain the plasmid until reaching mid-log (~OD 0.3). Cultures were crosslinked with formaldehyde, quenched with glycine, and 50 mL cell pellets were harvested. Pellets were sonicated in a Covaris Misonix sonicator for 16 min (20% duty factor, 75 PIP, 200 cycles per burst, 6°C) to achieve ~100-500 bp fragments and immunoprecipitation of HaloTagged-SigAb protein was performed according to Promega HaloChIP protocol. Before IP, 1/10 of each sample was saved as input control. Input control and HT-enriched samples were prepared for Illumina sequencing using NEBNext Ultra II Library Prep Kit for Illumina (NEB; E7645S) following manufacturer's protocol and sequenced on Illumina NovaSeq 6000 2x150 with the UW-Madison Biotechnology Center at ~10 million reads per sample.

ChIP-seq paired end FASTQ files were filtered to remove low quality bases using Trimmomatic (72) (v0.3) (Sliding window of 3:30, Minimum length of 36 bp, leading and trailing both a value of 3) and aligned to the *Acinetobacter baumannii* ATCC 17978 genome (GCA_001077675.1) using Bowtie2 (v2.2.2) (73) and default parameters. Samtools (v1.2) (74) and Picard Tools (v1.98) (75) were used to convert the SAM file to a sorted BAM file. Deeptools (v3.5.1) (76) was used to generate IP vs INPUT ratio files for visualization (binsize of 1 and readCount scaleFactorsMethod). ChIP-seq peaks were identified with the IP and INPUT BAM files using MACS3 (v3.0.0) (77) with default parameters except for using the "nomodel" option and 128 for the "extsize" and all for the "keep-dup" values.

RNA-sequencing. RNA-sequencing (RNA-seq) was performed on *A. baumannii* ATCC 17978 strains harboring either a *sigAb* overexpression (OE) vector (sJMP3382) or an empty vector control (sJMP3380). Cells were diluted 1:100 from a saturated overnight into AbRDM + kan to

maintain the plasmid and grown up shaking at 37°C. Once reaching mid-log (OD 0.3), 1 mM IPTG was added to induce expression, and cell pellets were collected for RNA purification at timepoints from 0 to 60 min after addition of IPTG. For *relA* OE experiments, *A. baumannii* ATCC 17978 strains containing *relA* OE vector (sJMP3790) or empty vector control (sJMP3719) were grown as described above, except cell pellets were collected for RNA purification at timepoints 0 and 10 min only.

Total RNA was extracted from *A. baumannii* using hot phenol organic extraction, as previously described (78). Briefly, mid-log cells were added to 1.25 mL stop solution (5% water-saturated phenol in ethanol), spun down at 11,000xg for 5 min at 4°C, and pellets were flash frozen in a dry ice:ethanol bath and stored at -80°C. Cells were lysed with lysozyme and SDS, total RNA was purified with phenol, phenol:chloroform, and chloroform extractions followed by ethanol precipitation, and residual DNA was removed with Turbo DNase I treatment (Invitrogen). Ribosomal RNA (rRNA) was depleted from the total RNA samples as previously described (79). Briefly, DNA oligos complementary to *A. baumannii* 23S, 16S, and 5S rRNA were annealed to the total RNA samples, RNase H treatment was performed to cleave the annealed rRNA, and the DNA oligos were removed with Turbo DNase I. rRNA-depleted samples were prepared for next-generation sequencing using NEBNext Ultra II Directional RNA Library Prep kit (NEB; E7765S) and NEBNext Multiplex Oligos for Illumina (NEB; E6640S). Libraries were sequenced on Illumina NovaSeq 6000 2x150 with the UW-Madison Biotechnology Center at ~10 million reads per sample.

Sequencing reads were trimmed using Trimmomatic (72) (version 0.39) (default parameters except for Sliding window of 3:30, Minimum length of 36 bp, leading and trailing both a value of 3) and mapped to the *A. baumannii* ATCC 17978 genome (GCA_001077675.1) using bwa-mem (80) (version 0.7.17-r1188) using default parameters. Mapped reads were further processed with Picard-tools (version 2.25.10) (CleanSAM and AddOrReplaceReadGroups) (75) and samtools (74) (version 1.2) (sort and index). Paired

aligned reads were mapped to genes with HTSeq (81) (version 0.6.0) with default parameters and normalized using FPKM as previously described (82, 83). The R package edgeR (84) (version 3.30.3) was used for differential gene expression analysis using Benjamini and Hochberg (85) adjusted P value (FDR) ≤ 0.05 as the significance threshold. Sequencing reads per gene were normalized using the fragments per kilobase per million mapped reads method (FPKM). Data were visualized in R using ggplot2.

CRISPRi knockdown experiments. sgRNAs targeting *sigAb* and *sabS* were cloned into pJMP2776 using oligos oJMP1243/oJMP1244 and oJMP2632/oJMP2633, respectively, as previously described to make pJMP3353 and pJMP3854 (86). The CRISPRi system was integrated into the att_{Tn7} site in *A. baumannii* ATCC 19606 (sJMP3329) using quad-parental mating and selection on gentamycin as previously described (87). *sigAb* knockdown strain (sJMP3363), *sabS* knockdown strain (sJMP3856), and non-targeting sgRNA strain (sJMP6498) were assayed for KD-dependent phenotypes by growing to saturation overnight in AbRDM, then pre-depleting by diluting 1:100 in AbRDM + 1mM IPTG for 4 hours (mid-log), and finally diluting 1:100 again in AbRDM + 1 mM IPTG + chemical (as indicated in figure legends) and measured OD_{600} for 16 or 18 hours in a Tecan Sunrise, Infinite Mplex, or Infinite Nano+ plate reader. Biolog phenotyping experiments were performed with the same pre-depletion method, except the final 1:100 diluted mid-log cells with 1 mM IPTG but no additional chemical were added to each well. Biolog Phenotype Microarray plates PM13 and PM16 were used.

SigAb induction phenotyping. SigAb promoter (P_{sigAb}) mScarlet-I reporter strain in *A. baumannii* ATCC 19606 (sJMP3406) and constitutive promoter (P_{lacUV5}) reporter strain (sJMP3402) were grown to saturation in LB. Saturated culture was diluted back 1:100 in AbRDM and grown up to mid-log. For Biolog Phenotype Microarray assays, 100 µL of cells diluted 1:100 in fresh AbRDM were added to each well of plates PM11, PM13, and PM16. For

620 copper testing, cells were diluted 1:100 into AbRDM supplemented with 150 µg/mL $CuSO_4$. 96-
621 well plates were grown in Tecan Infinite Mplex or Nano+ plate readers and measured OD_{600} and
622 red fluorescence.
623
624 **SigAb-AabA-AabB structural predictions.** Structural interactions between σ^{Ab}, AabA, and
625 AabB were predicted using Alphafold2 multimer (88) run on the COSMIC2 cloud platform with
626 the following parameters: Database: full_dbs, Model: multimer, Number of predictions per
627 model: 1, Latest date (YYYY-mm-dd) to use for template search: 2023-05-30, Models to relax:
628 none. Interactions between 1) SigAb and AabA or 2) AabA and AabB were predicted separately.
629 Multimer models containing AabA used either a cytoplasmic (modeled with σ^{Ab}) or periplasmic
630 (modeled with AabB) fragment based on the location of a predicted transmembrane helix
631 (residues 42-64, predicted by TMHMM 2.0 (89)). A predicted signal peptide in AabB (residues 1-
632 21, predicted by SignalP 6.0 (90), was removed prior to modeling. σ^{Ab} sequences corresponding
633 to σ_{R2} and σ_{R4} were predicted using InterProScan (91).
634
635 **Anti-SigAb phenotyping.** *In A. baumannii*: *aabA*, *aabB*, or *aabA-aabB*, were cloned into
636 pJMP3352 under control of the promoter P_{trc} according to "construction/notes" in Table S2 to
637 make plasmids pJMP3603, pJMP3604, and pJMP3549, respectively. Plasmids, including empty
638 vector pJMP3352, were mated into P_{sigAb} mRFP reporter strain (sJMP3602) to make strains
639 sJMP3629, sJMP3630, sJMP3631, and sJMP3380. Strains were grown overnight to saturation
640 in AbRDM supplemented with kan and 1 mM IPTG. OD_{600} and red fluorescent protein were
641 measured in a Tecan Infinite Mplex plate reader.
642 *In E. coli*: *aabA*, *aabB*, *aabA-aabB*, or *aabA*-cytoplasmic domain were cloned into
643 pJMP10740 under control of the promoter P_{araBAD} according to "construction/notes" in Table S2
644 to make plasmids pJMP3802, pJMP3803, pJMP3804, and pJMP3805, respectively. Plasmids
645 were co-mated into BW25113 P_{sigAb} mRFP reporter strain (sJMP3821) with *sigAb*

overexpression plasmid (pJMP3735) to make strains sJMP3822, sJMP3823, sJMP3824, and sJMP3825. Strains were grown overnight to saturation in AbRDM supplemented with kan, spec, 50 µM IPTG, and 10 mM L-arabinose. OD_{600} and red fluorescent protein were measured in a Tecan Infinite Mplex plate reader.

Targeted Tn-seq (CRISPRt) experiments. SigAb operon complementation strains were constructed by amplifying the *sigAb* gene with oJMP2344/2345 and the *sigAb* operon with oJMP2344/2347, assembling into SpeI/AscI-digested pJMP8602 to make pJMP3607 and pJMP3609, and using conjugation with selection on apramycin to integrate into the att_{Tn7} site in *A. baumannii* ATCC 17978 (sJMP3348), resulting in sJMP3624 and sJMP3628.

CRISPRt guides were designed to have a “CN” PAM with the spacer being 32 nt. CRISPRt gRNA library targeting the *A. baumannii* genes *rpoN*, *rpoD*, *rpoH*, *mdcD*, *sigAb*, *aabA*, and *aabB* was constructed as follows. An oPool (oJMP2322) containing guides targeting the first 4 genes (15 guides per gene) was amplified using oligos oJMP463/oJMP464 using low-cycle PCR as described above. An oPool (oJMP2143) containing 50 gRNAs targeting the *sigAb* operon was amplified using oligos oJMP463/oJMP464 and oJMP465/oJMP466 using the same PCR conditions. PCR products were spin-purified, quantified with nanodrop, and pooled together to achieve approximately equal gRNA ratios. Pooled product was digested with BsaI, ligated into BsaI-digested pJMP10621, and transformed into the mating strain to make sJMP3576 containing the CRISPRt plasmid library.

CRISPRt targeted transposition experiment was performed using tri-parental mating overnight at 30°C of: CRISPRt libarary (sJMP3576), CRISPRt helper plasmid (sJMP10275), and recipient strains 1) WT *A. baumannii* (sJMP3348), 2) *sigAb* gene complementation (sJMP3624), or 3) *sigAb* operon complementation (sJMP3628) with selection on apramycin to create strains sJMP3693, sJMP3694, and sJMP3696, respectively. Colonies were scraped off of 150mm plates (~5,000 colonies per strain) using LB and a cell scraper and gDNA was extracted. Tn-seq

library was prepared for Illumina sequencing as previously described (49). Briefly, gDNA was cut with MmeI enzyme, adaptor oligos oJMP1995/oJMP1996 were annealed and ligated to the DNA, and a low-cycle PCR was performed with oligos oJMP1997/oJMP1998. Samples were sequenced on Illumina NovaSeq 6000 2x150 with the UW-Madison Biotechnology Center at ~10 million reads per sample.

CRISPRt FASTQ files containing the transposon sequence (R1 FASTQ files) were trimmed to remove the transposon sequence using Cutadapt (v3.4) (92). Resulting reads longer than 40 nts were removed using fastp from Deeptools (v3.5.1) (76). Bowtie (v1.0.0) (93) was used to align the reads ≤ 40 nts using default parameters. Samtools (v1.2) (74) was used to convert the SAM file to a sorted BAM file and Deeptools (v3.5.1) (76) was used to generate BigWig files for visualization. Unique hits aligning to either strand were identified using Samtools (v1.2) and the standard Linux commands of awk, sort, and uniq to filter the alignment file to count aligned reads on the forward or reverse strands.

Data Availability. Raw data will be deposited to the National Center for Biotechnology Information Sequencing Read Archive (SRA) under BioProject (### pending). All other data is available upon request.

Acknowledgements

This work was supported by the National Institutes of Health under award numbers K22AI137122 and 1R35GM150487-01. We thank the UW-Madison Biotechnology Center Illumina Pilot Grant Program for providing funding for sequencing. We thank Lauren Palmer and members of Peters lab for helpful comments.

Competing Interest

None.

References

1. McConnell MJ, Actis L, Pachón J. 2013. Acinetobacter baumannii: human infections, factors contributing to pathogenesis and animal models. FEMS Microbiol Rev 37:130-55.
2. CDC. 2019. Antibiotic resistance threats in the United States, 2019.
3. Lupo A, Haenni M, Madec JY. 2018. Antimicrobial Resistance in Acinetobacter spp. and Pseudomonas spp. Microbiol Spectr 6.
4. Abdi SN, Ghotaslou R, Ganbarov K, Mobed A, Tanomand A, Yousefi M, Asgharzadeh M, Kafil HS. 2020. Acinetobacter baumannii Efflux Pumps and Antibiotic Resistance. Infect Drug Resist 13:423-434.
5. Bonnin RA, Poirel L, Nordmann P. 2012. AbaR-type transposon structures in Acinetobacter baumannii, p 234-6, J Antimicrob Chemother, vol 67, England.
6. Kornelsen V, Kumar A. 2021. Update on Multidrug Resistance Efflux Pumps in Acinetobacter spp. Antimicrob Agents Chemother 65:e0051421.
7. Gruber TM, Gross CA. 2003. Multiple sigma subunits and the partitioning of bacterial transcription space. Annu Rev Microbiol 57:441-66.
8. Staroń A, Sofia HJ, Dietrich S, Ulrich LE, Liesegang H, Mascher T. 2009. The third pillar of bacterial signal transduction: classification of the extracytoplasmic function (ECF) sigma factor protein family. Mol Microbiol 74:557-81.
9. Braun V, Mahren S, Ogierman M. 2003. Regulation of the FecI-type ECF sigma factor by transmembrane signalling. Curr Opin Microbiol 6:173-80.
10. Donohue TJ. 2019. Shedding light on a Group IV (ECF11) alternative σ factor. Mol Microbiol 112:374-384.
11. Mecsas J, Rouviere PE, Erickson JW, Donohue TJ, Gross CA. 1993. The activity of sigma E, an Escherichia coli heat-inducible sigma-factor, is modulated by expression of outer membrane proteins. Genes Dev 7:2618-28.
12. Paget MS. 2015. Bacterial Sigma Factors and Anti-Sigma Factors: Structure, Function and Distribution. Biomolecules 5:1245-65.
13. Koo BM, Rhodius VA, Nonaka G, deHaseth PL, Gross CA. 2009. Reduced capacity of alternative sigmas to melt promoters ensures stringent promoter recognition. Genes Dev 23:2426-36.
14. Erickson JW, Gross CA. 1989. Identification of the sigma E subunit of Escherichia coli RNA polymerase: a second alternate sigma factor involved in high-temperature gene expression. Genes Dev 3:1462-71.
15. Wang QP, Kaguni JM. 1989. A novel sigma factor is involved in expression of the rpoH gene of Escherichia coli. J Bacteriol 171:4248-53.
16. Lima S, Guo MS, Chaba R, Gross CA, Sauer RT. 2013. Dual molecular signals mediate the bacterial response to outer-membrane stress. Science 340:837-41.
17. De Las Peñas A, Connolly L, Gross CA. 1997. The sigmaE-mediated response to extracytoplasmic stress in Escherichia coli is transduced by RseA and RseB, two negative regulators of sigmaE. Mol Microbiol 24:373-85.
18. Rhodius VA, Suh WC, Nonaka G, West J, Gross CA. 2006. Conserved and variable functions of the sigmaE stress response in related genomes. PLoS Biol 4:e2.
19. Rhodius VA, Mutalik VK, Gross CA. 2012. Predicting the strength of UP-elements and full-length E. coli σE promoters. Nucleic Acids Res 40:2907-24.
20. Guo MS, Updegrove TB, Gogol EB, Shabalina SA, Gross CA, Storz G. 2014. MicL, a new σE-dependent sRNA, combats envelope stress by repressing synthesis of Lpp, the major outer membrane lipoprotein. Genes Dev 28:1620-34.
21. Schulz S, Eckweiler D, Bielecka A, Nicolai T, Franke R, Dötsch A, Hornischer K, Bruchmann S, Düvel J, Häussler S. 2015. Elucidation of sigma factor-associated

networks in Pseudomonas aeruginosa reveals a modular architecture with limited and function-specific crosstalk. PLoS Pathog 11:e1004744.
22. Firoved AM, Boucher JC, Deretic V. 2002. Global genomic analysis of AlgU (sigma(E))-dependent promoters (sigmulon) in Pseudomonas aeruginosa and implications for inflammatory processes in cystic fibrosis. J Bacteriol 184:1057-64.
23. Mathur J, Davis BM, Waldor MK. 2007. Antimicrobial peptides activate the Vibrio cholerae sigmaE regulon through an OmpU-dependent signalling pathway. Mol Microbiol 63:848-58.
24. Kovacikova G, Skorupski K. 2002. The alternative sigma factor sigma(E) plays an important role in intestinal survival and virulence in Vibrio cholerae. Infect Immun 70:5355-62.
25. Casella LG, Weiss A, Pérez-Rueda E, Antonio Ibarra J, Shaw LN. 2017. Towards the complete proteinaceous regulome of Acinetobacter baumannii. Microb Genom 3:mgen000107.
26. Robinson A, Brzoska AJ, Turner KM, Withers R, Harry EJ, Lewis PJ, Dixon NE. 2010. Essential biological processes of an emerging pathogen: DNA replication, transcription, and cell division in Acinetobacter spp. Microbiol Mol Biol Rev 74:273-97.
27. Geisinger E, Mortman NJ, Vargas-Cuebas G, Tai AK, Isberg RR. 2018. A global regulatory system links virulence and antibiotic resistance to envelope homeostasis in Acinetobacter baumannii. PLoS Pathog 14:e1007030.
28. Palethorpe S, Farrow JM, 3rd, Wells G, Milton ME, Actis LA, Cavanagh J, Pesci EC. 2022. Acinetobacter baumannii Regulates Its Stress Responses via the BfmRS Two-Component Regulatory System. J Bacteriol 204:e0049421.
29. Bai J, Dai Y, Farinha A, Tang AY, Syal S, Vargas-Cuebas G, van Opijnen T, Isberg RR, Geisinger E. 2021. Essential Gene Analysis in Acinetobacter baumannii by High-Density Transposon Mutagenesis and CRISPR Interference. J Bacteriol 203:e0056520.
30. Green ER, Fakhoury JN, Monteith AJ, Pi H, Giedroc DP, Skaar EP. 2022. Bacterial hydrophilins promote pathogen desiccation tolerance. Cell Host Microbe 30:975-987.e7.
31. Juttukonda LJ, Green ER, Lonergan ZR, Heffern MC, Chang CJ, Skaar EP. 2019. Acinetobacter baumannii OxyR Regulates the Transcriptional Response to Hydrogen Peroxide. Infect Immun 87.
32. Valentine SC, Contreras D, Tan S, Real LJ, Chu S, Xu HH. 2008. Phenotypic and molecular characterization of Acinetobacter baumannii clinical isolates from nosocomial outbreaks in Los Angeles County, California. J Clin Microbiol 46:2499-507.
33. Kelley LA, Mezulis S, Yates CM, Wass MN, Sternberg MJE. 2015. The Phyre2 web portal for protein modeling, prediction and analysis. Nature Protocols 10:845-858.
34. Fang C, Li L, Shen L, Shi J, Wang S, Feng Y, Zhang Y. 2019. Structures and mechanism of transcription initiation by bacterial ECF factors. Nucleic Acids Res 47:7094-7104.
35. Browning DF, Busby SJ. 2016. Local and global regulation of transcription initiation in bacteria. Nat Rev Microbiol 14:638-50.
36. Cashel M, Gallant J. 1969. Two compounds implicated in the function of the RC gene of Escherichia coli. Nature 221:838-41.
37. Hauryliuk V, Atkinson GC, Murakami KS, Tenson T, Gerdes K. 2015. Recent functional insights into the role of (p)ppGpp in bacterial physiology. Nat Rev Microbiol 13:298-309.
38. Barker MM, Gaal T, Josaitis CA, Gourse RL. 2001. Mechanism of regulation of transcription initiation by ppGpp. I. Effects of ppGpp on transcription initiation in vivo and in vitro. J Mol Biol 305:673-88.
39. Kröger C, MacKenzie KD, Alshabib EY, Kirzinger MWB, Suchan DM, Chao TC, Akulova V, Miranda-CasoLuengo AA, Monzon VA, Conway T, Sivasankaran SK, Hinton JCD, Hokamp K, Cameron ADS. 2018. The primary transcriptome, small RNAs and regulation

of antimicrobial resistance in Acinetobacter baumannii ATCC 17978. Nucleic Acids Res 46:9684-9698.

40. Daniels DL, Urh M. 2013. Isolation of intracellular protein--DNA complexes using HaloCHIP, an antibody-free alternative to chromatin immunoprecipitation. Methods Mol Biol 977:111-24.
41. Arndt D, Grant JR, Marcu A, Sajed T, Pon A, Liang Y, Wishart DS. 2016. PHASTER: a better, faster version of the PHAST phage search tool. Nucleic Acids Res 44:W16-21.
42. Dar D, Sorek R. 2018. High-resolution RNA 3'-ends mapping of bacterial Rho-dependent transcripts. Nucleic Acids Res 46:6797-6805.
43. Maharjan RP, Sullivan GJ, Adams FG, Shah BS, Hawkey J, Delgado N, Semenec L, Dinh H, Li L, Short FL, Parkhill J, Paulsen IT, Barquist L, Eijkelkamp BA, Cain AK. 2023. DksA is a conserved master regulator of stress response in Acinetobacter baumannii. Nucleic Acids Res 51:6101-6119.
44. Chaba R, Alba BM, Guo MS, Sohn J, Ahuja N, Sauer RT, Gross CA. 2011. Signal integration by DegS and RseB governs the σ E-mediated envelope stress response in Escherichia coli. Proc Natl Acad Sci U S A 108:2106-11.
45. Maillard AP, Girard E, Ziani W, Petit-Härtlein I, Kahn R, Covès J. 2014. The crystal structure of the anti-σ factor CnrY in complex with the σ factor CnrH shows a new structural class of anti-σ factors targeting extracytoplasmic function σ factors. J Mol Biol 426:2313-27.
46. Gallagher LA, Ramage E, Weiss EJ, Radey M, Hayden HS, Held KG, Huse HK, Zurawski DV, Brittnacher MJ, Manoil C. 2015. Resources for Genetic and Genomic Analysis of Emerging Pathogen Acinetobacter baumannii. J Bacteriol 197:2027-35.
47. Tripathi S, Voogdt CGP, Bassler SO, Anderson M, Huang PH, Sakenova N, Capraz T, Jain S, Koumoutsi A, Bravo AM, Trotter V, Zimmerman M, Sonnenburg JL, Buie C, Typas A, Deutschbauer AM, Shiver AL, Huang KC. 2024. Randomly barcoded transposon mutant libraries for gut commensals I: Strategies for efficient library construction. Cell Rep 43:113517.
48. Parker DJ, Demetci P, Li GW. 2019. Rapid Accumulation of Motility-Activating Mutations in Resting Liquid Culture of Escherichia coli. J Bacteriol 201.
49. Banta AB, Myers KS, Ward RD, Cuellar RA, Place M, Freeh CC, Bacon EE, Peters JM. 2024. A Targeted Genome-scale Overexpression Platform for Proteobacteria. bioRxiv.
50. Barchinger SE, Ades SE. 2013. Regulated proteolysis: control of the Escherichia coli σ(E)-dependent cell envelope stress response. Subcell Biochem 66:129-60.
51. Todor H, Osadnik H, Campbell EA, Myers KS, Li H, Donohue TJ, Gross CA. 2020. Rewiring the specificity of extracytoplasmic function sigma factors. Proc Natl Acad Sci U S A 117:33496-33506.
52. Helmann JD. 2002. The extracytoplasmic function (ECF) sigma factors. Adv Microb Physiol 46:47-110.
53. Sureka K, Dey S, Datta P, Singh AK, Dasgupta A, Rodrigue S, Basu J, Kundu M. 2007. Polyphosphate kinase is involved in stress-induced mprAB-sigE-rel signalling in mycobacteria. Mol Microbiol 65:261-76.
54. Baruzzo G, Serafini A, Finotello F, Sanavia T, Cioetto-Mazzabò L, Boldrin F, Lavezzo E, Barzon L, Toppo S, Provvedi R, Manganelli R, Di Camillo B. 2023. Role of the Extracytoplasmic Function Sigma Factor SigE in the Stringent Response of Mycobacterium tuberculosis. Microbiology Spectrum 0:e02944-22.
55. Hamrock FJ, Ryan D, Shaibah A, Ershova AS, Mogre A, Sulimani MM, Reichardt S, Hokamp K, Westermann AJ, Kröger C. 2023. Global analysis of the RNA-RNA interactome in Acinetobacter baumannii AB5075 uncovers a small regulatory RNA repressing the virulence-related outer membrane protein CarO. bioRxiv:2023.12.04.569942.

56. Al Ali A, Alsulami J, Aubee JI, Idowu A, Tomlinson BR, Felton EA, Jackson JK, Kennedy SJ, Torres NJ, Shaw LN, Thompson KM. 2023. Staphylococcus aureus SigS Induces Expression of a Regulatory Protein Pair That Modulates Its mRNA Stability. J Bacteriol 205:e0039222.
57. Falcone M, Ferrara S, Rossi E, Johansen HK, Molin S, Bertoni G. 2018. The Small RNA ErsA of Pseudomonas aeruginosa Contributes to Biofilm Development and Motility through Post-transcriptional Modulation of AmrZ. Front Microbiol 9:238.
58. Johansen J, Rasmussen AA, Overgaard M, Valentin-Hansen P. 2006. Conserved small non-coding RNAs that belong to the sigmaE regulon: role in down-regulation of outer membrane proteins. J Mol Biol 364:1-8.
59. Murdoch CC, Skaar EP. 2022. Nutritional immunity: the battle for nutrient metals at the host-pathogen interface. Nat Rev Microbiol 20:657-670.
60. Palmer LD, Skaar EP. 2016. Transition Metals and Virulence in Bacteria. Annu Rev Genet 50:67-91.
61. Giachino A, Waldron KJ. 2020. Copper tolerance in bacteria requires the activation of multiple accessory pathways. Mol Microbiol 114:377-390.
62. Alquethamy SF, Khorvash M, Pederick VG, Whittall JJ, Paton JC, Paulsen IT, Hassan KA, McDevitt CA, Eijkelkamp BA. 2019. The Role of the CopA Copper Efflux System in Acinetobacter baumannii Virulence. Int J Mol Sci 20.
63. Williams CL, Neu HM, Alamneh YA, Reddinger RM, Jacobs AC, Singh S, Abu-Taleb R, Michel SLJ, Zurawski DV, Merrell DS. 2020. Characterization of Acinetobacter baumannii Copper Resistance Reveals a Role in Virulence. Front Microbiol 11:16.
64. Moraleda-Muñoz A, Marcos-Torres FJ, Pérez J, Muñoz-Dorado J. 2019. Metal-responsive RNA polymerase extracytoplasmic function (ECF) sigma factors. Mol Microbiol 112:385-398.
65. Iruegas R, Pfefferle K, Göttig S, Averhoff B, Ebersberger I. 2023. Feature architecture aware phylogenetic profiling indicates a functional diversification of type IVa pili in the nosocomial pathogen Acinetobacter baumannii. PLoS Genet 19:e1010646.
66. Katoh K, Misawa K, Kuma Ki, Miyata T. 2002. MAFFT: a novel method for rapid multiple sequence alignment based on fast Fourier transform. Nucleic Acids Research 30:3059-3066.
67. Price MN, Dehal PS, Arkin AP. 2010. FastTree 2--approximately maximum-likelihood trees for large alignments. PLoS One 5:e9490.
68. Tonkin-Hill G, Lees JA, Bentley SD, Frost SDW, Corander J. 2019. Fast hierarchical Bayesian analysis of population structure. Nucleic Acids Res 47:5539-5549.
69. Crooks GE, Hon G, Chandonia JM, Brenner SE. 2004. WebLogo: a sequence logo generator. Genome Res 14:1188-90.
70. Bacon EE, Tran JS, Nadig N, Peters JM. 2024. Modular, inducible, and titratable expression systems for Escherichia coli and Acinetobacter baumannii. bioRxiv.
71. Ng HH, Robert F, Young RA, Struhl K. 2003. Targeted recruitment of Set1 histone methylase by elongating Pol II provides a localized mark and memory of recent transcriptional activity. Mol Cell 11:709-19.
72. Bolger AM, Lohse M, Usadel B. 2014. Trimmomatic: a flexible trimmer for Illumina sequence data. Bioinformatics 30:2114-20.
73. Langmead B, Salzberg SL. 2012. Fast gapped-read alignment with Bowtie 2. Nat Methods 9:357-9.
74. Li H, Handsaker B, Wysoker A, Fennell T, Ruan J, Homer N, Marth G, Abecasis G, Durbin R. 2009. The Sequence Alignment/Map format and SAMtools. Bioinformatics 25:2078-9.
75. Institute B. 2019. Picard Toolkit. https://github.com/broadinstitute/picard. Accessed

76. Ramírez F, Ryan DP, Grüning B, Bhardwaj V, Kilpert F, Richter AS, Heyne S, Dündar F, Manke T. 2016. deepTools2: a next generation web server for deep-sequencing data analysis. Nucleic Acids Res 44:W160-5.
77. Zhang Y, Liu T, Meyer CA, Eeckhoute J, Johnson DS, Bernstein BE, Nusbaum C, Myers RM, Brown M, Li W, Liu XS. 2008. Model-based analysis of ChIP-Seq (MACS). Genome Biol 9:R137.
78. Khodursky AB, Bernstein JA, Peter BJ, Rhodius V, Wendisch VF, Zimmer DP. 2003. Escherichia coli spotted double-strand DNA microarrays: RNA extraction, labeling, hybridization, quality control, and data management. Methods Mol Biol 224:61-78.
79. Duan Y, Sun Y, Ambros V. 2020. RNA-seq with RNase H-based ribosomal RNA depletion specifically designed for C. elegans. MicroPubl Biol 2020.
80. Li H, Durbin R. 2009. Fast and accurate short read alignment with Burrows-Wheeler transform. Bioinformatics 25:1754-60.
81. Anders S, Pyl PT, Huber W. 2015. HTSeq--a Python framework to work with high-throughput sequencing data. Bioinformatics 31:166-9.
82. Zhang Y, Myers KS, Place M, Serate J, Xie D, Pohlmann E, La Reau A, Landick R, Sato TK. 2022. Transcriptomic Data Sets for Zymomonas mobilis 2032 during Fermentation of Ammonia Fiber Expansion (AFEX)-Pretreated Corn Stover and Switchgrass Hydrolysates. Microbiol Resour Announc 11:e0056422.
83. Lakey BD, Myers KS, Alberge F, Mettert EL, Kiley PJ, Noguera DR, Donohue TJ. 2022. The essential Rhodobacter sphaeroides CenKR two-component system regulates cell division and envelope biosynthesis. PLoS Genet 18:e1010270.
84. Robinson MD, McCarthy DJ, Smyth GK. 2010. edgeR: a Bioconductor package for differential expression analysis of digital gene expression data. Bioinformatics 26:139-40.
85. Benjamini Y, Hochberg Y. 2018. Controlling the False Discovery Rate: A Practical and Powerful Approach to Multiple Testing. Journal of the Royal Statistical Society: Series B (Methodological) 57:289-300.
86. Banta AB, Ward RD, Tran JS, Bacon EE, Peters JM. 2020. Programmable Gene Knockdown in Diverse Bacteria Using Mobile-CRISPRi. Curr Protoc Microbiol 59:e130.
87. Ward RD, Tran JS, Banta AB, Bacon EE, Rose WE, Peters JM. 2024. Essential gene knockdowns reveal genetic vulnerabilities and antibiotic sensitivities in Acinetobacter baumannii. mBio 15:e0205123.
88. Evans R, O'Neill M, Pritzel A, Antropova N, Senior A, Green T, Žídek A, Bates R, Blackwell S, Yim J, Ronneberger O, Bodenstein S, Zielinski M, Bridgland A, Potapenko A, Cowie A, Tunyasuvunakool K, Jain R, Clancy E, ..., Hassabis D. 2021. Protein complex prediction with AlphaFold-Multimer. bioRxiv.
89. Krogh A, Larsson B, von Heijne G, Sonnhammer EL. 2001. Predicting transmembrane protein topology with a hidden Markov model: application to complete genomes. J Mol Biol 305:567-80.
90. Teufel F, Almagro Armenteros JJ, Johansen AR, Gíslason MH, Pihl SI, Tsirigos KD, Winther O, Brunak S, von Heijne G, Nielsen H. 2022. SignalP 6.0 predicts all five types of signal peptides using protein language models. Nature Biotechnology 40:1023-1025.
91. Zdobnov EM, Apweiler R. 2001. InterProScan--an integration platform for the signature-recognition methods in InterPro. Bioinformatics 17:847-8.
92. Martin M. 2011. Cutadapt removes adapter sequences from high-throughput sequencing reads. 2011 17:3.
93. Langmead B. 2010. Aligning short sequencing reads with Bowtie. Curr Protoc Bioinformatics Chapter 11:Unit 11.7.
94. Peters JM, Koo BM, Patino R, Heussler GE, Hearne CC, Qu J, Inclan YF, Hawkins JS, Lu CHS, Silvis MR, Harden MM, Osadnik H, Peters JE, Engel JN, Dutton RJ, Grossman

AD, Gross CA, Rosenberg OS. 2019. Enabling genetic analysis of diverse bacteria with Mobile-CRISPRi. Nat Microbiol 4:244-250.

95. Chakravartty V, Cronan JE. 2015. A series of medium and high copy number arabinose-inducible Escherichia coli expression vectors compatible with pBR322 and pACYC184. Plasmid 81:21-6.

96. Stabb EV, Ruby EG. 2002. RP4-based plasmids for conjugation between Escherichia coli and members of the Vibrionaceae. Methods Enzymol 358:413-26.

97. Hall AN, Hall BW, Kinney KJ, Olsen GG, Banta AB, Noguera DR, Donohue TJ, Peters JM. 2023. Tools for Genetic Engineering and Gene Expression Control in Novosphingobium aromaticivorans and Rhodobacter sphaeroides. bioRxiv.

98. Campbell EA, Tupy JL, Gruber TM, Wang S, Sharp MM, Gross CA, Darst SA. 2003. Crystal structure of Escherichia coli sigmaE with the cytoplasmic domain of its anti-sigma RseA. Mol Cell 11:1067-78.

Figure 1. SigAb is an *Acinetobacter*-specific σ factor.

A Alignment of ECF σ factors from SigAb ortholog search across the γ-proteobacteria. Alignment is colored by protein sequence identity, with darker blue indicating greater amino acid conservation. The Moraxellales family contains *Acinetobacter* species. **B** Phylogenetic tree based on alignment from (a). SigAb orthologs are in red and RpoE orthologs are in gold. An additional ECF distinct from SigAb and RpoE present in non-*baumannii Acinetobacters* is in blue. Outer ring denotes γ-proteobacterial taxonomic order, and inner ring distinguishes between different *Acinetobacter* sp. classifications, including the *A. calcoaceticus-baumannii* (ACB) complex.

Figure 2. Identification of core promoter sequence recognized by SigAb.

A mRFP fluorescent reporter to assay *sigAb* promoter (P_{sigAb}) activity. Reporter is stably integrated in the chromosome in the att_{Tn7} site. *aabA* and *aabB* encoded downstream of *sigAb* are predicted to be in an operon. **B and C** P_{sigAb}-*mrfp* reporter activity in WT or *sigAb* overexpression strains in (b) *A. baumannii* or (c) *E. coli*. Promoter activity is calculated as absorbance units (AU) normalized to OD_{600} and the no promoter control (n=3). Data are represented as the mean ± s.d. and significance was calculated with a two-tailed Student's *t*-test ($p<0.05$). **D** Systematic mutagenesis of P_{sigAb} sequence. TSS was identified using 5' RACE. Point mutations in promoter were assayed for activity using mRFP reporter. Heatmap shown is median of n=5 assays for 1-13 biological replicates per mutation. **E** Quantification of P_{sigAb} mutagenesis data from (d) as an activity logo.

Figure 3. SigAb directly controls a small regulon.

A Sequence alignment of the SigAb-dependent promoter motifs for *sigAb*, *sabS*, and *relA*. Stars indicate conserved bases and +1 indicates the putative transcription start site (TSS). **B** ChIP-seq peak at *sigAb* locus from an *A. baumannii* strain harboring HaloTagged SigAb. Data are

represented as log_2(fold change) of immunoprecipitated sample normalized to input control. Peak calling algorithm was used for significant peak identification. **C** ChIP-seq peak at the *relA* locus. **D** ChIP-seq peak at an intergenic region containing an uncharacterized sRNA, *sabS*. **E** P_{sabS}-*mrfp* and P_{relA}-*mrfp* reporter activity in WT or *sigAb* overexpression strains in *A. baumannii*. Relative promoter activity is calculated as absorbance units (AU) normalized to OD_{600} and the no promoter control (n=3). Data are represented as the mean ± s.d. and significance was calculated with a two-tailed Student's *t*-test ($p<0.05$).

Figure 4. SigAb indirectly affects global transcription.

A RNA-sequencing experimental overview. RNA was harvested and sequenced from *A. baumannii* strains harboring an inducible *sigAb* overexpression vector or empty vector control as a time course (0 to 60 minutes post-induction). **B** Number of significantly upregulated genes ($Log_2FC > 1$) after induction of SigAb overexpression compared to empty vector control. RNA-seq was performed in duplicate and a false discovery rate (FDR) cutoff of 0.05 was used. **C** Table of gene set enrichments for genes significantly upregulated after 5 min of induction. **D** Heatmap of efflux pumps and resistance genes significantly upregulated ($Log_2FC > 1$, FDR < 0.05, T=5 min) in RNA-seq time course experiment. Genes displayed are members of the efflux and transporter-related STRING clusters CL:4901 and CL:4700. Operons are denoted to the right, with arrows indicating direction of transcription.

Figure 5. SigAb mitigates and responds to copper stress.

A Heatmap of heavy metal resistance genes significantly upregulated ($Log_2FC > 1$, FDR < 0.05, T=10 min) in RNA-seq time course experiment of *sigAb* overexpression strain compared to empty vector control. Operons are denoted to the right, with arrows indicating direction of transcription. **B** Growth curves plotted as OD_{600} over time (hr) of CRISPRi *sigAb* knockdown (KD) strain and non-targeting (NT) control in rich defined medium with 250 μg/mL $CuSO_4$ stress

(n=3). Data are represented as mean ± s.d. for NT control with no stress (red), *sigAb* KD with no stress (blue), NT control with copper stress (green), and *sigAb* KD with copper stress (purple). **C** *sigAb* KD growth defects in metal stresses graphed as area under the curve (AUC) normalized to NT control (n=2-9). Data are represented as the mean ± s.d. and significance was calculated with a two-tailed Student's *t*-test ($p<0.05$). Bars without asterisks are not significantly different from the control **D** SigAb induction curves plotted as P_{sigAb} activity (mRFP fluorescence) vs. cell density (OD_{600}) for metal and antibiotic stress conditions using Biolog Phenotype Microarray PM13.

Figure 6. AabA and AabB have antisigma activity.

A SigAb-AabA-AabB structural interaction model. Model predicted using AlphaFold2 run on COSMIC2 cloud platform. SigAb (σ^{Ab}) region 2 (R2) and region 4 (R4) were predicted using InterProScan and AabA transmembrane domain was predicted by TMHMM 2.0. **B** Comparison of (left) *A. baumannii* σ^{Ab}-AabA interaction model to (right) *C. metallidurans* CnrH-CnrY and *E. coli* σ^{E}-RseA crystal structures (98, 45). AabA spans across the σ^{Ab} R2 and R4 regions, similar to CnrH-CnrY, while RseA and MucA are found in between σ^{E} R2 and R4. **C** mRFP reporter assay for P_{sigAb} activity in *A. baumannii* strains harboring overexpression vectors with *aabA*, *aabB*, both *aabA* and *aabB*, or an empty vector control. Promoter activity is calculated as absorbance units (AU) normalized to OD_{600} (n=3). Data are represented as the mean ± s.d. and significance was calculated with a two-tailed Student's *t*-test ($p<0.05$).

Figure 7. Targeted Tn-seq reveals that the *sigAb* operon is required for fitness in rich medium.

A Schematic of CRISPR-guided targeted transposition (CRISPRt) system for gene knockouts. A high-density CRISPRt library targeting across several genes was constructed and used for gene essentiality testing. **B** CRISPRt insertions (Normalized Tn-seq reads) within the *rpoN* (non-

essential) or *rpoD* (essential) genes are shown as green bars on a linear scale. Read counts are cut off at 20,000 reads due to over-representation of some insertion sites (> 250,000 reads). **C** CRISPRt insertions within the *sigAb* operon in either WT *A. baumannii* (green), a strain harboring *sigAb* gene duplication in att_{Tn7} site (pink), or a strain harboring *sigAb* operon duplication in att_{Tn7} site (blue). Normalized Tn-seq reads are shown on a linear scale with read counts cut off at 20,000 reads due to over-representation of some insertion sites (> 600,000 reads).

Figure 1

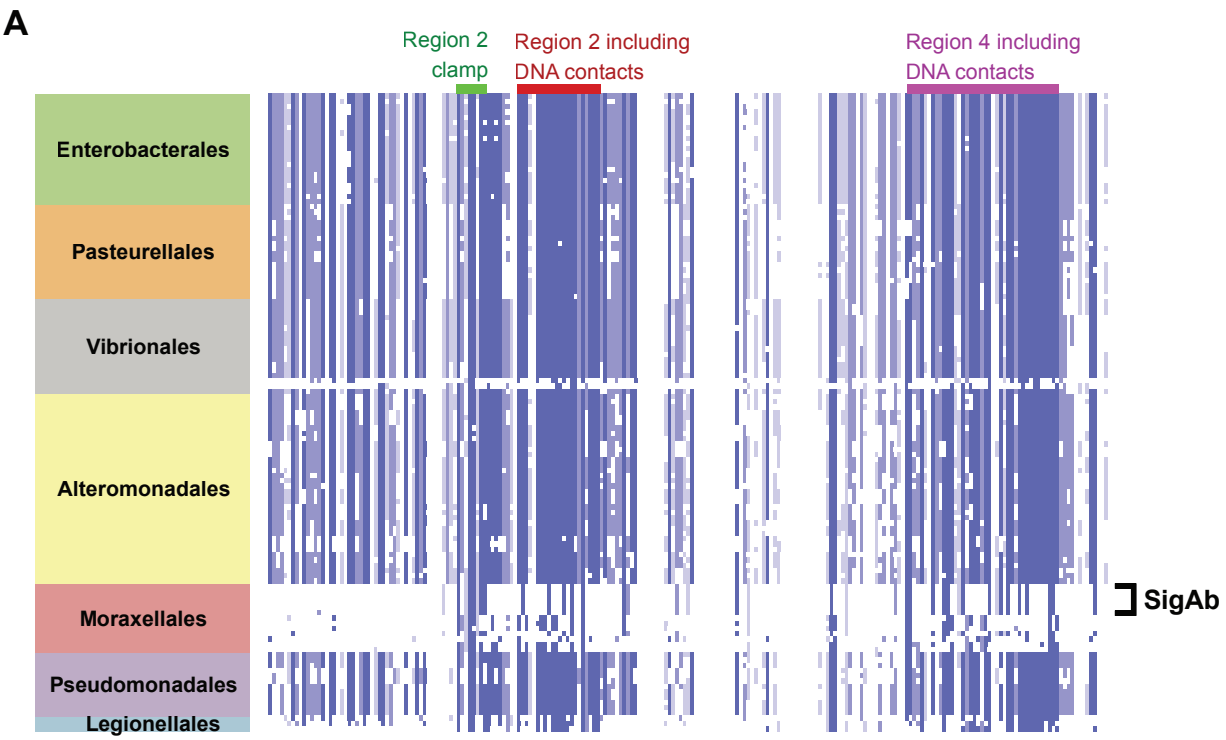
A
Region 2 clamp
Region 2 including DNA contacts
Region 4 including DNA contacts
Enterobacterales
Pasteurellales
Vibrionales
Alteromonadales
Moraxellales
Pseudomonadales
Legionellales
SigAb

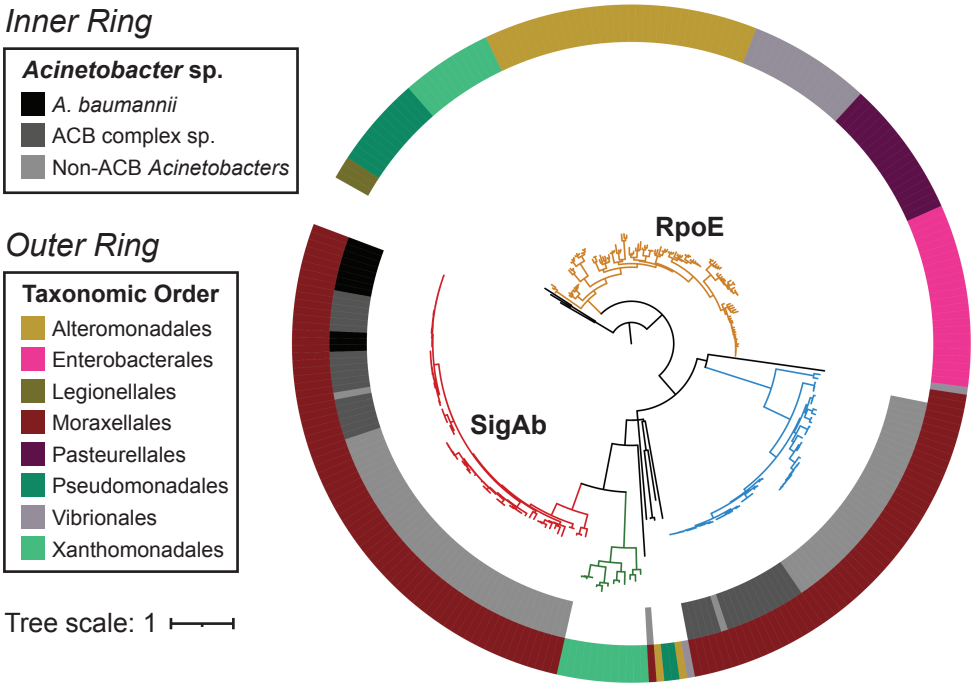
B
Inner Ring
Acinetobacter sp.
A. baumannii
ACB complex sp.
Non-ACB Acinetobacters
Outer Ring
Taxonomic Order
Alteromonadales
Enterobacterales
Legionellales
Moraxellales
Pasteurellales
Pseudomonadales
Vibrionales
Xanthomonadales
Tree scale: 1
RpoE
SigAb

Figure 2

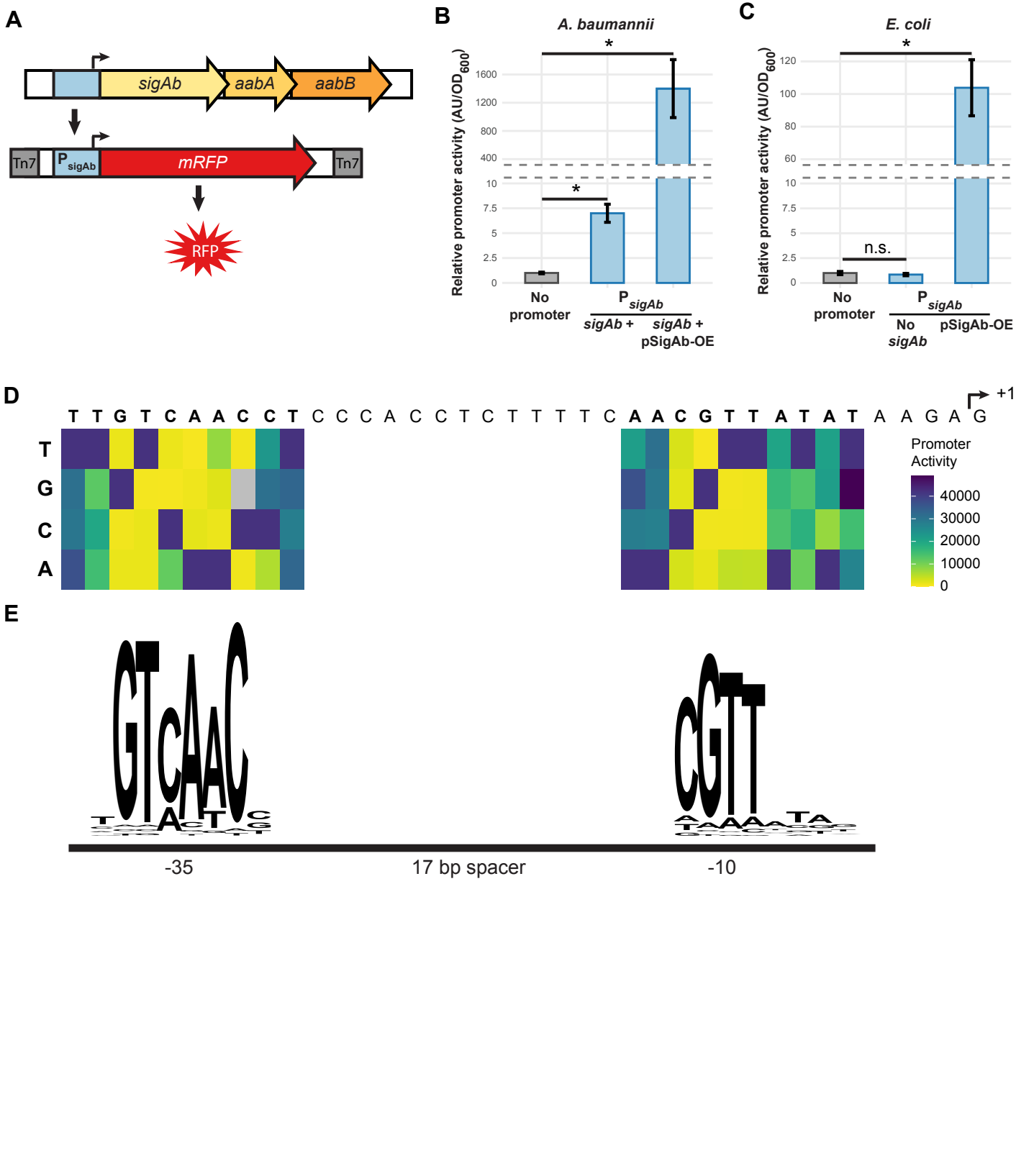
A
sigAb
aabA
aabB
Tn7
P sigAb
mRFP
Tn7
RFP
B
A. baumannii
Relative promoter activity (AU/OD600)
1600
1200
800
400
10
7.5
5
2.5
0
*
*
No promoter
P sigAb
sigAb +
sigAb + pSigAb-OE
C
E. coli
Relative promoter activity (AU/OD600)
120
100
80
60
10
7.5
5
2.5
0
*
n.s.
No promoter
P sigAb
No sigAb
pSigAb-OE
D
T T G T C A A C C T C C C A C C T C T T T T C A A C G T T A T A T A A G A G
+1
T
G
C
A
Promoter Activity
40000
30000
20000
10000
0
E
-35
17 bp spacer
-10

Figure 3

A

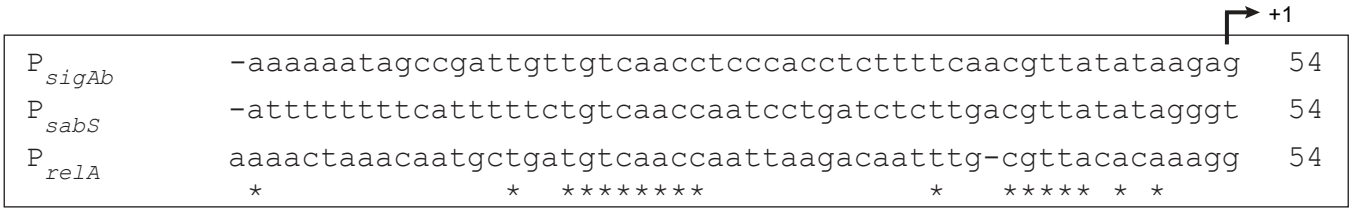

B

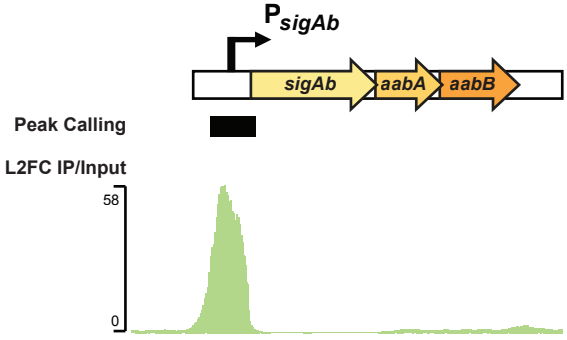

C

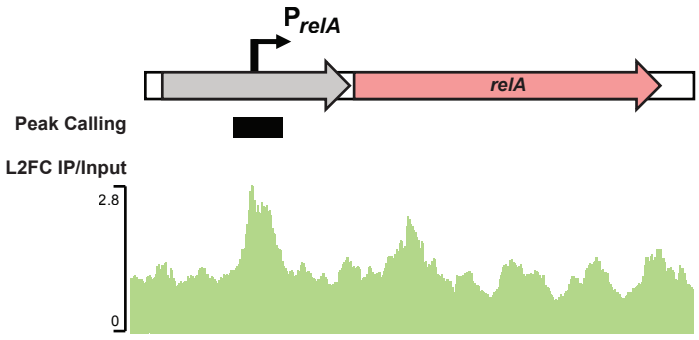

D

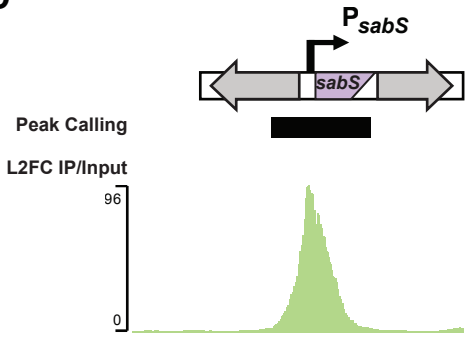

E

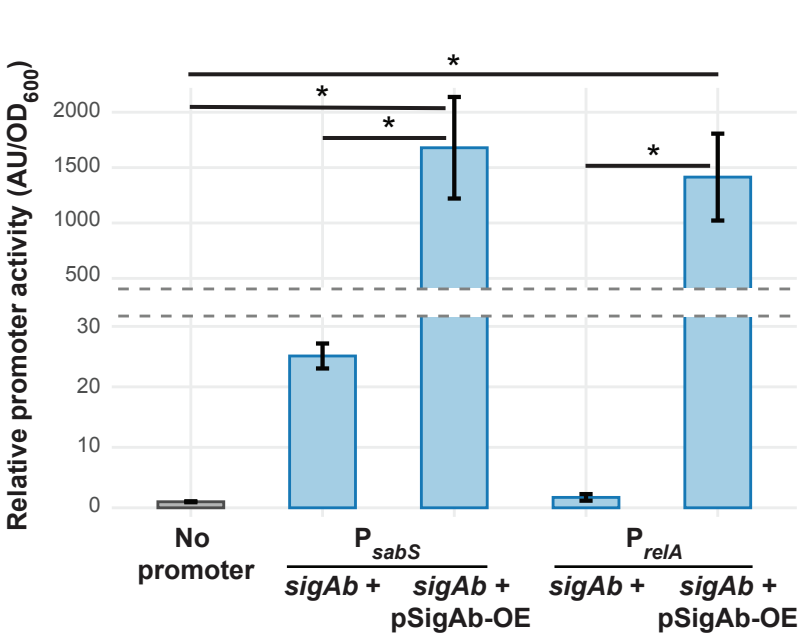

Figure 4

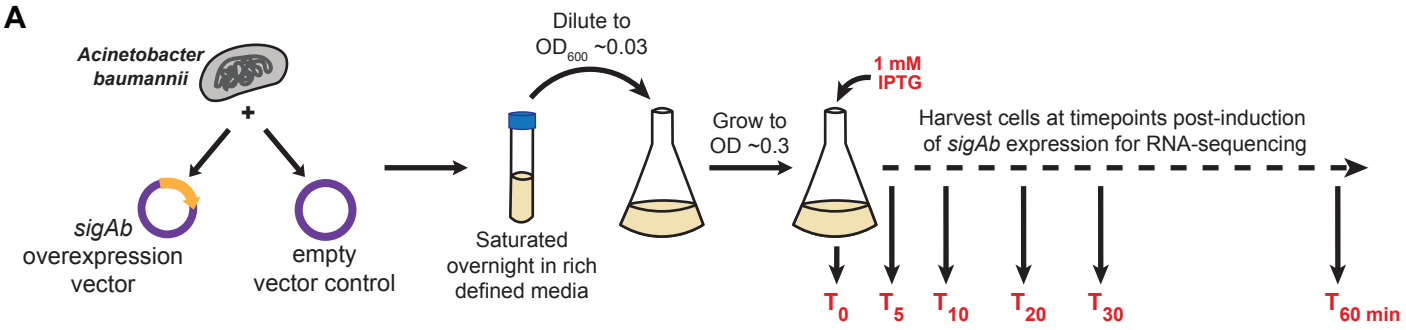

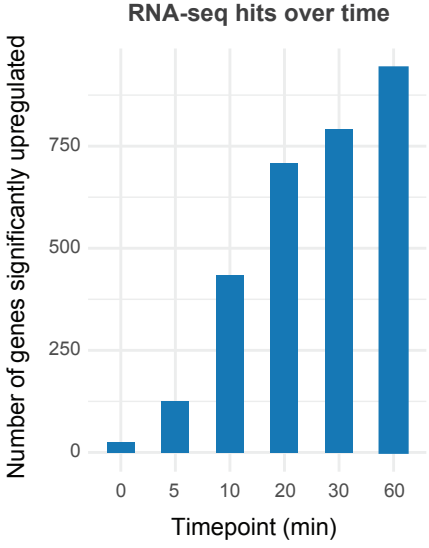

C

Significant hits after 5 min of *sigAb* overexpression

Group Description	STRING Cluster	# Genes
Metabolism and oxidoreductase activity	CL:1579	33
Prophages†	---	20
Membrane and regulation of cellular process	CL:3469	11
Efflux transporter and HlyD family secretion protein	CL:4901	9
ABC transporters and sulfur metabolism	CL:4700	7
Nitrogen compound metabolic process	CL:98	8
TetR family regulatory proteins and amino acid transport	CL:5960	6
LysR family regulatory proteins	CL:6384	4
Putative sRNA‡	---	3
Hydrolase activity	CL:5413	2
Potassium ion transport and electron transport chain	CL:5548	2
Nitrogen metabolism	CL:3230	2
Other	---	18
Total		125

† Prophages predicted using Phaster (41)

‡ sRNA defined as RNA-seq signal next to motif hit in inter or intragenic region

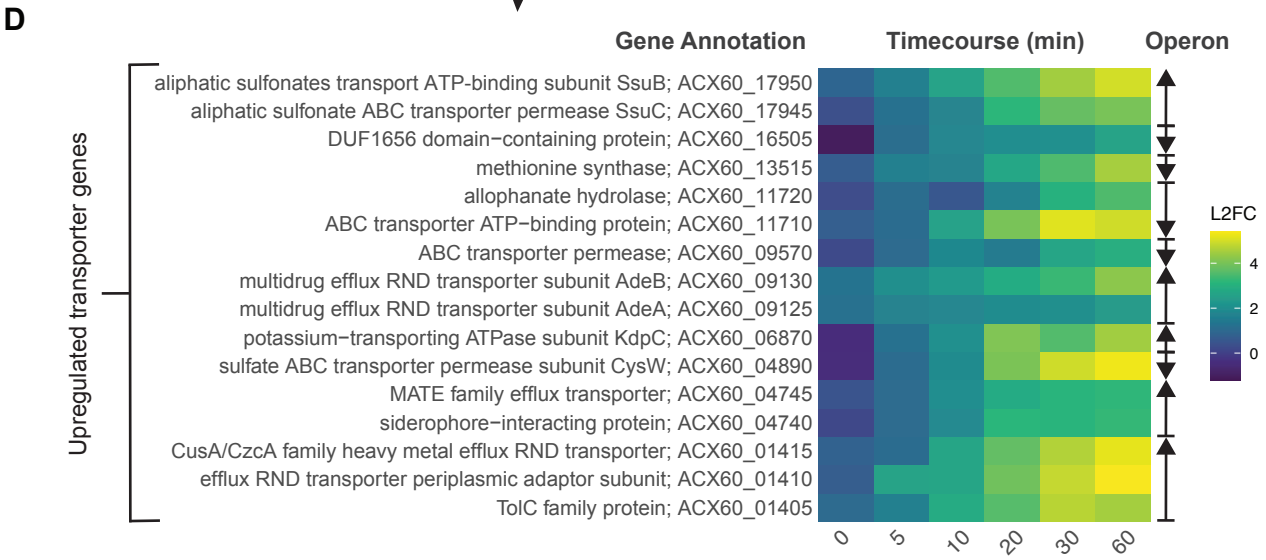

Figure 5

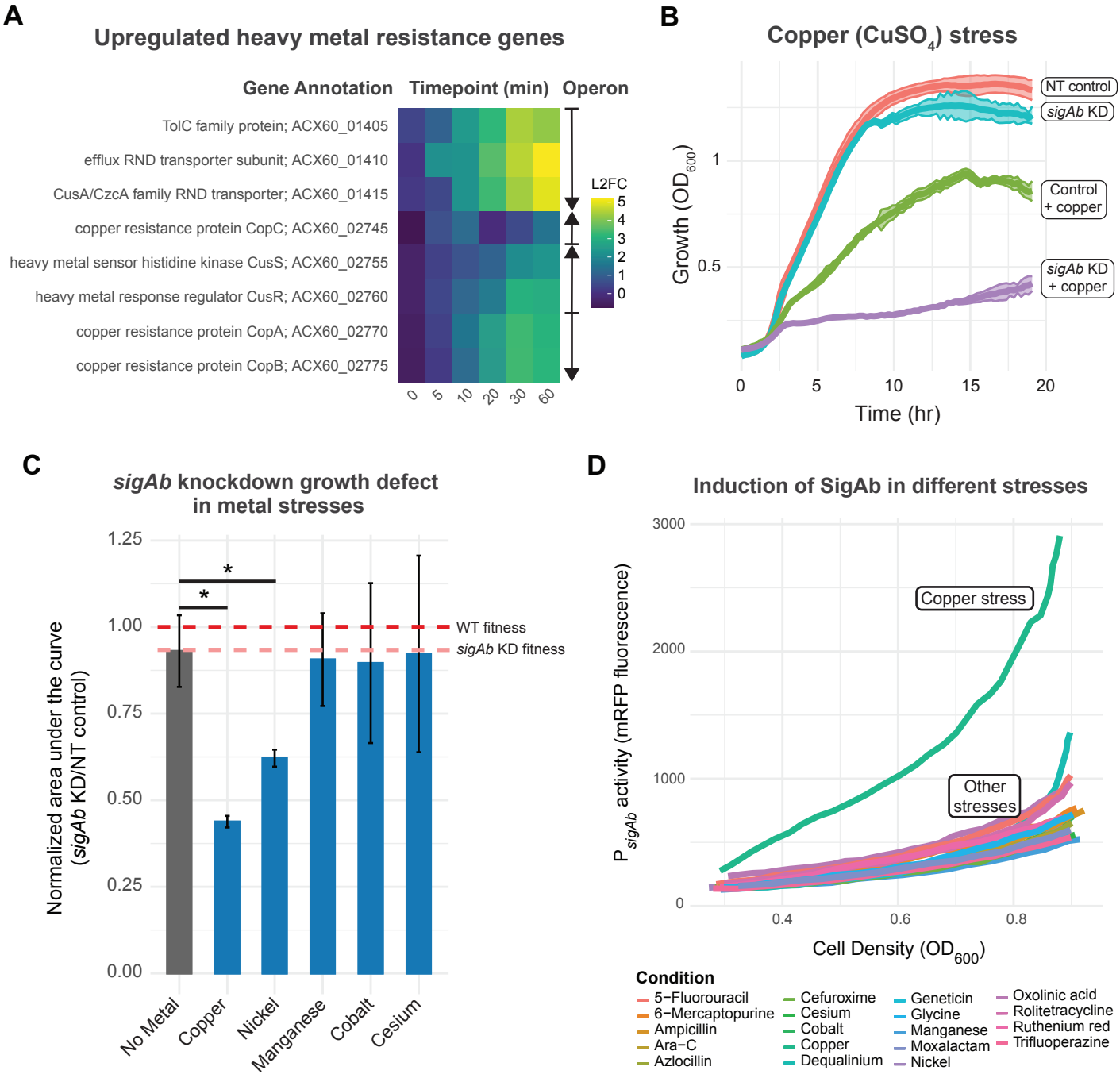
A
Upregulated heavy metal resistance genes
Gene Annotation
Timepoint (min)
Operon
TolC family protein; ACX60_01405
efflux RND transporter subunit; ACX60_01410
CusA/CzcA family RND transporter; ACX60_01415
copper resistance protein CopC; ACX60_02745
heavy metal sensor histidine kinase CusS; ACX60_02755
heavy metal response regulator CusR; ACX60_02760
copper resistance protein CopA; ACX60_02770
copper resistance protein CopB; ACX60_02775
0 5 10 20 30 60
L2FC
5 4 3 2 1 0
B
Copper (CuSO4) stress
Growth (OD600)
1
0.5
0 5 10 15 20
Time (hr)
NT control
sigAb KD
Control + copper
sigAb KD + copper
C
sigAb knockdown growth defect in metal stresses
Normalized area under the curve (sigAb KD/NT control)
1.25
1.00
0.75
0.50
0.25
0.00
*
*
WT fitness
sigAb KD fitness
No Metal
Copper
Nickel
Manganese
Cobalt
Cesium
D
Induction of SigAb in different stresses
P sigAb activity (mRFP fluorescence)
3000
2000
1000
0
0.4 0.6 0.8
Cell Density (OD600)
Copper stress
Other stresses
Condition
5−Fluorouracil
6−Mercaptopurine
Ampicillin
Ara−C
Azlocillin
Cefuroxime
Cesium
Cobalt
Copper
Dequalinium
Geneticin
Glycine
Manganese
Moxalactam
Nickel
Oxolinic acid
Rolitetracycline
Ruthenium red
Trifluoperazine

Figure 6

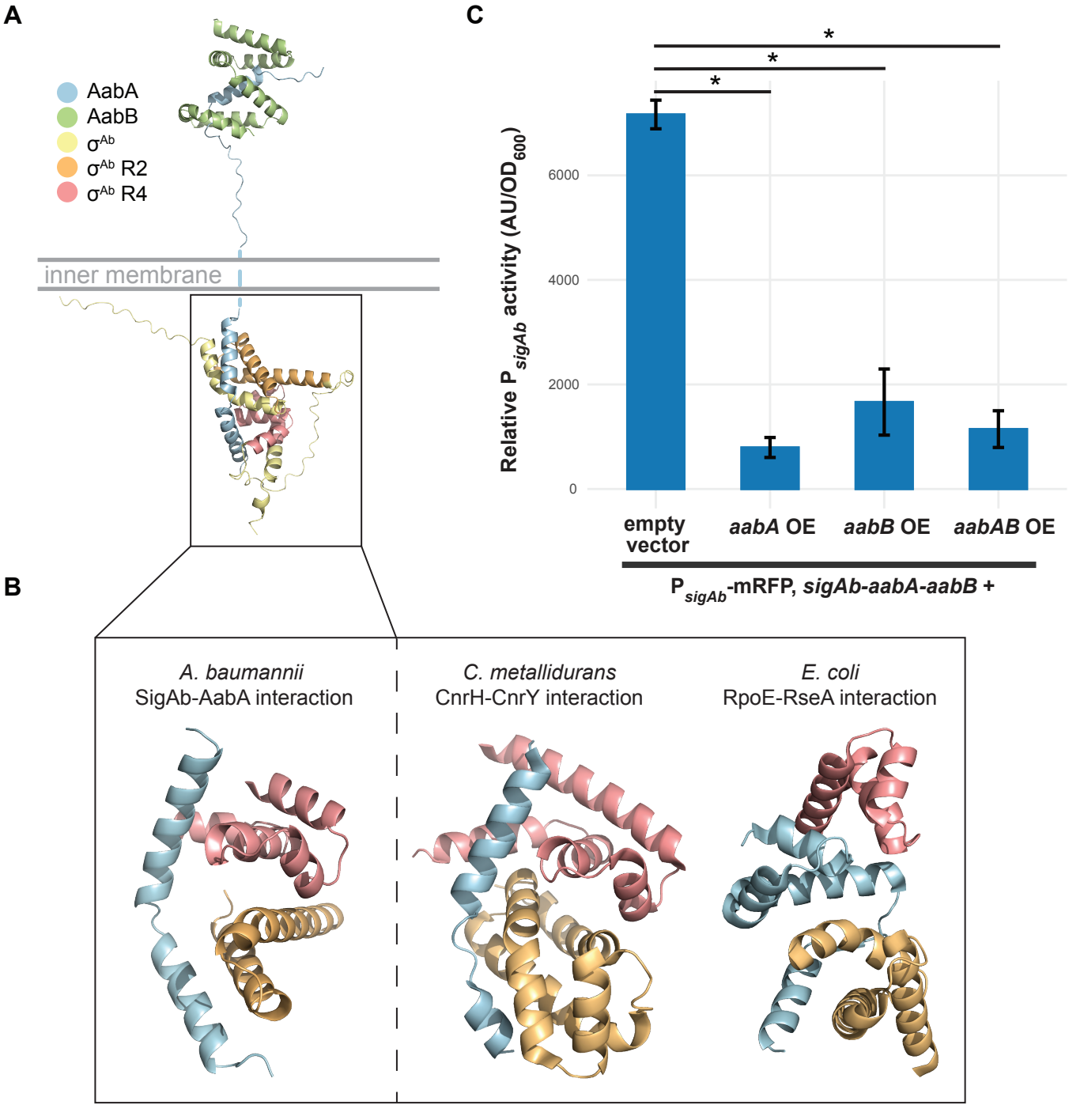
A
AabA
AabB
σ^Ab
σ^Ab R2
σ^Ab R4
inner membrane
C
Relative P sigAb activity (AU/OD600)
6000
4000
2000
0
*
*
*
empty vector
aabA OE
aabB OE
aabAB OE
P sigAb-mRFP, sigAb-aabA-aabB +
B
A. baumannii
SigAb-AabA interaction
C. metallidurans
CnrH-CnrY interaction
E. coli
RpoE-RseA interaction

Figure 7

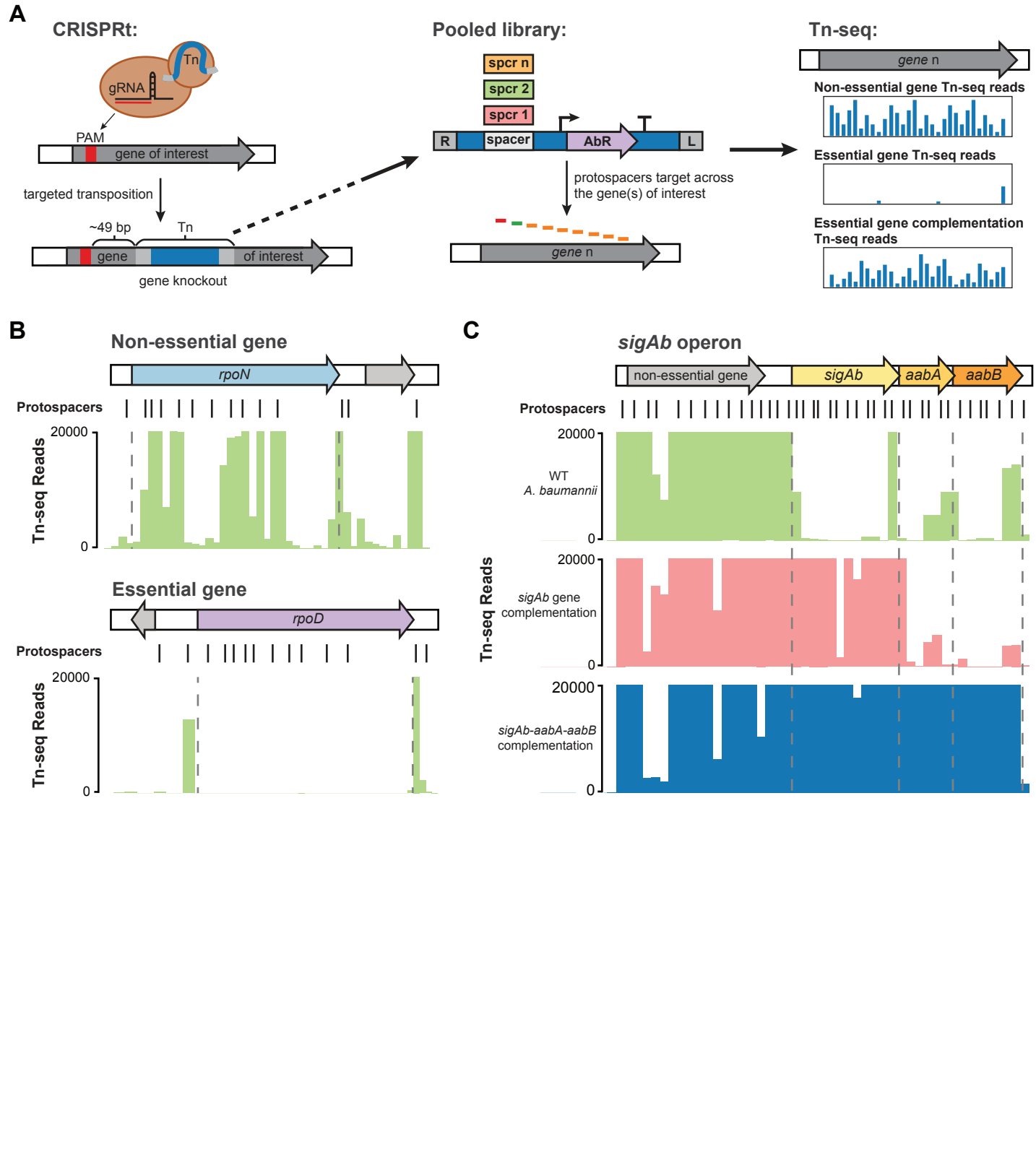
A
CRISPRt:
Tn
gRNA
PAM
gene of interest
targeted transposition
~49 bp
Tn
gene
of interest
gene knockout
Pooled library:
spcr n
spcr 2
spcr 1
R
spacer
AbR
L
protospacers target across the gene(s) of interest
gene n
Tn-seq:
gene n
Non-essential gene Tn-seq reads
Essential gene Tn-seq reads
Essential gene complementation Tn-seq reads
B
Non-essential gene
rpoN
Protospacers
Tn-seq Reads
20000
0
Essential gene
rpoD
Protospacers
Tn-seq Reads
20000
0
C
sigAb operon
non-essential gene
sigAb
aabA
aabB
Protospacers
Tn-seq Reads
20000
WT
A. baumannii
0
20000
sigAb gene complementation
0
20000
sigAb-aabA-aabB complementation
0